Carbon Fibre Buckle Arrestors for Offshore Pipelines

Mahmoud Alrsai [1], Hassan Karampour [1,*], Wayne Hall[1], Alex k. Lindon[1] and Faris Albermani[2]

[1]Griffith School of Engineering and Built Environment, Griffith University, Gold Coast Campus, QLD 4222, Australia.

[2]School of Engineering and Technology, Central Queensland University, QLD 4740, Australia.

*Corresponding author: h.karampour@griffith.edu.au

Abstract

Feasibility and efficiency of using carbon fibre reinforced polymer (CFRP) buckle arrestors in steel offshore pipelines with *D/t* of 28 and 40 are investigated using hyperbaric chamber tests. CFRP arrestors are manufactured using Prepreg (PP), Wet-Layup (WL) and Vacuum Bagging (VB) curing methods, with coarse and fine sand surface preparations. A parametric study is performed that outlines the performance of CFRP arrestors in various geometric configurations. Efficiency of CFRP arrestors using different manufacturing methods and various geometric configurations are calculated and compared with those of conventional steel buckle arrestors. It is shown that the efficiencies of CFRP arrestors vary between 0.74 and 1.0 for different manufacturing methods. Optimum efficiencies are obtained in the WL technique, using fine sanding, with CFRP arrestor of thickness twice the steel pipe-wall thickness, and fibres oriented in the hoop direction. Results show that at similar efficiencies, the CFRP arrestors can be much thinner than conventional slip-on or integral arrestors.

Keywords

Offshore pipelines; buckle propagation; buckle arrestor; collapse under external pressure; carbon fibre; composites

1. Introduction

A major concern in design of subsea pipelines in deep and ultra-deep waters is the collapse under external hydrostatic pressure. In the presence of local damage in the pipe-wall (in the form of out-of-roundness, dents or corrosion) local collapse can be initiated in the pipeline. The hazardous subsea pipeline accidents caused by corrosion, 65% were because of external corrosion, many researchers have investigated the collapse of subsea pipelines due to corrosion [1-4]. Once local collapse initiated, the circular cross-section of the pipe transforms into a dog-bone shape, and eventually a flat shape (causing shutdown of the pipeline), as the buckle

rapidly propagates along the pipeline [5-10]. The corresponding local collapse due to external pressure may be coupled with other loadings in the pipeline, such as bending and axial force, resulting in buckle interaction [11-15].

The lowest pressure required to perpetuate the local buckle is termed propagation pressure (P_P), which is typically only 15% of the collapse pressure (P_{CO}). In case the external pressure exceeds the propagation buckle criterion [16], buckle arrestors are installed at certain intervals along the pipeline based on cost and spare pipe philosophy. Such arrestors are snuggly fitted around the pipeline to limit the damage and safeguard the downstream section of the pipeline [17-19].

Existing buckle arrestors are made of stiff metal rings which locally augment the circumferential stiffness of the pipeline, and thus hinder the buckle propagation. A buckle arrestor can halt the buckle completely, or may allow the buckle to cross-over at a higher pressure. The buckle arrestor pressure capacity (P_X) is closely related to the length L, thickness h and yield stress σ_{ya} of the arrestor as well as diameter D, wall thickness t, and yield stress σ_y of the pipe . The efficiency of a buckle arrestor (η), is defined as [21]

$$\eta = \frac{P_X - P_P}{P_{CO} - P_P} \tag{1}$$

where P_P and P_{CO} are the propagation and collapse pressures of the adjacent pipe, respectively. An efficiency of 1.0 ($P_X = P_{CO}$) is achievable, if the buckle can be arrested in the upstream section of the pipeline. Most common types of buckle arrestors are: (1) slip-on arrestors [19], where the arrestor is slipped over the pipe, (2) integral arrestors [18], where the arrestor is welded to the pipe, (3) spiral arrestors [20], in which the arrestor is wound onto the pipe, and (4) clamped arrestor [22]. Amongst those, slip-on arrestors and integral arrestors are more prevalent. Slip-on arrestors are normally preferred to integral arrestors, since no welding is required. However, previous research has shown that their efficiency is normally lower than the integral arrestors [22]. The integral arrestor is a thick ring that is welded onto the pipeline. The weld should be robust enough to resist large deformations during the buckle propagation [18,23]. Therefore, the costs of installation of integral arrestors are significantly higher than other options.

Due to its excellent properties, such as high specific strength and stiffness, performance to weight ratio, thermal stability and corrosion resistance [24-27], carbon fibre reinforced polymer (CFRP) wraps are used to repair corroded and mechanically damaged offshore pipelines [28-30]. Moreover, experimental and numerical investigations have proved that the application of CFRP in pipeline repair improves the capacity of the damaged pipeline in carrying bending, compression, tension and torsional loads, in both quasi-static and cyclic loading scenarios [31-32].

The common buckle arrestors may hinder the pipe laying operation. For instance, in reel-lay method the pre-installed devices (such as buckle arrestors) interfere with the reeling and unreeling process [31]. Moreover, current buckle arrestors cannot be used in the inner components of pipe-in-pipe systems and pipeline bundles [6, 7, 34, 35]. The current study proposes a CFRP buckle arrestor and investigates its feasibility, efficiency and appropriateness in offshore pipelines. The current work complements a previous study by the current authors [36] which proved the feasibility of the CFRP buckle arrestor concept. To do so, experiments are conducted on stainless steel pipelines with diameter-to-thickness ratio, D/t, of 28 and 40, without arrestors (bare samples) and with CFRP arrestors, in a hyperbaric chamber. A parametric study is conducted to find the optimum thickness (h), length (L), and orientation ($\theta°$) of the CFRP arrestor. Moreover, different CFRP arrestor manufacturing methods are tested. Using the experimental results, efficiency of CFRP arrestor is calculated and compared against those of existing buckle arrestors.

2. Materials and methods

2.1 Material properties

The Pipeline

The hyperbaric chamber tests were conducted on small-scale seamless, SS-304 pipelines with D/t ratios of 28 and 40. Mechanical properties of each pipe used in the experiments were measured using uni-axial tensile tests conducted on coupon samples cut from each batch (6 meters long) of the pipes, and along their longitudinal direction according to the recommendations of AS 1391-2007 [37]. The hyperbaric chamber tests showed different buckle propagation speeds in the pipes with different D/t ratio. Therefore, the coupon tests were conducted at two different strain-rates; slow rate (such that rupture in the sample occurs in 4-5 minutes) and fast rate (8 times the slow rate). The tests were paused at the vicinity of the yield and ultimate points, to capture the upper and lower yield and ultimate stresses,

respectively. The forces were calculated directly from the INSTRON 5900 universal testing system, and the strains were measured using a clip-on extensometer with a gauge length of 50.8 mm, attached to the middle section of the coupon sample. The ends of the coupon samples were flattened before being clamped into the machine. In order to account for the curved coupon surface, the correction factor recommended in AS 1391-2007 [37] was used. Detail of the coupon samples and strain rates are given in Table 1.

CFRP arrestors

Coupon samples according to ASTM d3039/D3039M-08 [38] were cut from the CFRP sheets. All the coupons were 25.0 mm wide by 250 mm long unidirectional beam laminates. The coupon samples had a thickness of 0.80-0.92 mm in the vacuum bagging samples (VB), 1.25-1.31 mm in wet lay-up samples (WL), and 0.86-0.95 mm in prepreg samples (PP). The samples were tested in the longitudinal (0°) and transverse (90°) directions. Average results of the coupon test for different manufacturing methods and corresponding volume fractions (V_f) are given in Table 2.

2.2 Manufacturing

The methods

The CFRP buckle arrestors were fabricated and installed using three manufacturing techniques: (1) the vacuum bagging (VB), (2) the wet lay-up (WL), and (3) the prepreg (PP).

In the VB technique, a weight ratio of 50% carbon fibre (UD, 200 g/m^2) to 50% resin was used to calculate the required amount of epoxy resin, taking into account a resin loss factor of 25%. The epoxy resin was made up of resin (R 170) and hardener (H 180) with a ratio of 5:1 of resin to hardener. The fibre layers were initially cut into the required length (L) and orientation (θ). A metal roller was then used for consolidation, and the resin was spread evenly and gradually (to avoid any voids). Then, the wet fibre layer was tightly wound around the pipe at the required location. The procedure was repeated until the required thickness (h) was achieved. Then, the vacuum bag was installed, and the CFRP arrestor was consolidated under 1 bar vacuum pressure and cured for 24 hours at room temperature. Fig. 1 shows a summary of the manufacturing process for the vacuum bagging technique.

In the WL technique, the same manufacturing process as in the VB was adopted. However, instead of using a vacuum bag, the samples were left to cure in the room temperature for 24 hours (Fig. 2).

In the PP method, the CFRP buckle arrestors were manufactured from unidirectional prepreg commercial epoxy resin (VTM62 HS200), with a spread rate of 200 g/m^2 [39]. The prepreg CFRP arrestors were manufactured by stacking the self-sticking layers to achieve the required thickness (h) and in the desired orientation (θ). Each layer of the prepreg had a thickness slightly over 0.2 mm. A shrink tube was wrapped over the arrestor and the samples were oven cured for 1 hour at a temperature of 120°C. The PP manufacturing method procedure is shown in Fig. 3.

In order to study the effect of the bond between the CFRP arrestor and the pipeline, two different surface preparation methods were implemented; (a) fine sanding (F) using a 180 grit sandpaper, and (b) coarse sanding (C) with a 40 grit sandpaper.

2.3 Samples and labelling

General

The tested pipelines are selected based on the D/t (slenderness ratio). The thicker pipeline has $D/t \approx 28$ (D = 25.4 mm and t = 0.9 mm) and the thinner pipeline has $D/t \approx 40$ (D = 63.5 mm and t = 1.6 mm). From each D/t, three batches (A, B and C) in length of 6 meters were purchased. From each batch, two or three pipelines were cut and were used to manufacture bare samples (without arrestors) or samples with CFRP arrestors. The samples are identified by their D/t (28 or 40), pipe batch label (A to E), coupon test ID (1 or 2), CFRP manufacturing method (VB, WL or PP) and surface preparation process (F or C). For example, sample 28A2WLF represents a pipeline with $D/t \approx 28$ (D = 25.4 mm and t = 0.9 mm), cut from batch A, coupon test 2, with CFRP manufactured using the wet layup method (WL), and surface prepared via fine sanding (F). The bare samples are identified with "BS". So, 40C1BS refers to a pipeline with $D/t \approx 40$ (D = 63.5 mm and t = 1.6 mm), cut from batch C, coupon test number 1, without any arrestors.

Parametric study

In the parametric study, 6 samples were prepared from the thick pipe ($D/t \approx 28$), all with CFRP arrestors manufactured using the PP method and fine sanding surface preparation. Different batches of steel (batch D and E) were used to manufacture the pipelines in the parametric study. In this case, a 28D1PPF1 represents a thick pipe ($D/t \approx 28$), from batch D, coupon test 1, manufactured with PP method and fine sanding, in CFRP configuration 1 (see Fig 5).

2.4 Quasi-static Hyperbaric chamber tests

Test setup

The samples were tested inside a hyperbaric chamber with an inner diameter of 176 mm and clear length of 4 m, with a nominal capacity of 30 MPa (water depth of 3,000 m) shown in Fig. 4. The pipeline samples were sealed at both ends by welding on a thick disc, placed inside the hyperbaric chamber and then filled with water. One end of the pipe was connected to an outlet nozzle through the chamber's wall and vented to the atmosphere. The pipe specimen was filled with water before being placed inside the chamber. The pipe was vented to the atmosphere using a tube and through an outlet in the chamber wall. The chamber was filled with water, sealed and pressurised at a slow rate using a high pressure pump. The change in the volume of the pipe during the test was monitored using a digital scale to measure the weight of the water exiting the pipe via the outlet in the chamber's wall as shown in Fig. 4. A buckle monitoring system comprised of DVU unit (DVU400-17) (Fig. 4b), and a high-pressure camera (Titan-3000) and LED light (C-DragonHP) were placed inside the chamber, to monitor the collapse and its propagation. The camera and LED assembly were secured inside the chamber, using a custom-made support made of acrylic. The chamber was then sealed and filled with water. The hyperbaric pressure time-history of the chamber was monitored using a pressure gauge shown in Fig. 4.

In order to control the location of the collapse in the pipeline, an initial imperfection in the shape of a dent was induced to one end of the pipe and at a distance of 6D from the bulkhead (the thick disc welded to the sample). To impose the dent, the pipeline was clamped in the jaw of a universal testing machine, and a rigid semi-circular rod of the same diameter was gradually pressed against it to produce an ovality ratio Δ_0 less than 1%. The imperfection was quantified by measuring the maximum and minimum diameters (D_{max} and D_{min}) of the dented pipe and represented in terms of ovality Δ_0

$$\Delta_0 = \frac{D_{\max} - D_{\min}}{D_{\max} + D_{\min}} \tag{2}$$

Test plans

In total 18 hyperbaric chamber tests were conducted comprising three testing series;

(1) Bare samples were tested to calculate the buckling behaviour and the propagation pressure (P_P) of the pipeline without arrestors. The results were used as benchmarks for the tests with CFRP arrestors. Two samples from each D/t with length of 2.5 meters each were tested, and their properties and obtained results are given in Table 3.

(2) A parametric study was conducted to find the optimum thickness (h), length (L), and orientation ($\theta°$) of the CFRP arrestor. A total of six tests were conducted on the pipeline with $D/t \approx 28$, using PP method with fine sanding. The CFRP buckle arrestor configurations are shown in Fig. 5 and their parametric properties are represented in Table 4. In configurations 1 and 2 (Fig. 5 from top), effect of the thickness of CFRP arrestors was studied. In configurations 3 and 4, two CFRP arrestors were oriented in θ = -35º/+35º and θ = -55º/+55º biaxial (with respect to the longitudinal pipeline axis), respectively, in order to investigate fibre orientation effect. The effect of the length of the CFRP arrestor (L) was studied by comparing configurations 1-2 and 5-6. All pipe samples had a length of 1.6 meters each.

(3) A total of eight hyperbaric chamber tests were conducted on samples with CFRP arrestors, to investigate the effect of the manufacturing technique and diameter to thickness ratio. Properties of the samples are outlined in Table 5. The pipe samples had lengths of 2.5 meters each.

3. Results and discussion

3.1 Material properties

The yield stresses (σ_y), modulus of elasticity (E), ultimate stresses (σ_u), and elongation at rupture of the SS-304 stainless steel coupon samples are given in Table 1. The stress-strain curves at two different strain rates are shown in Fig. 6. The elongation at rupture is calculated by dividing the gauge length of the coupon sample before the test and at the rupture (drop in the load shown in Fig. 6), and is represented in percentage in Table 1. The high elongations at rupture show that the stainless steel has a large ductility. The thinner pipe ($D/t \approx 40$) is more ductile than the thick pipe ($D/t \approx 28$). The average differences between the upper and lower stress (shown with superscripts U and L in Table 1, respectively) at the yield and at the ultimate stress are 1.2% and 1.9%, respectively.

The moduli of elasticity of the samples are independent of the strain rate. However, the characteristic stresses upsurge with an increase in the strain rate (increase in the speed of the tensile test). Particularly, the lower yield stress is more sensitive to the strain rate compared to other characteristic stress values. Elongations at rupture (ductility) of the samples seem to decrease with an increase in the strain rate.

The modulus of elasticity (E), ultimate stress (σ_u) and corresponding volume fraction (V_f) of the CFRP coupon samples are given in Table 2 for three manufacturing techniques and in two fibre

orientations. The average moduli of elasticity of the CFRP along the direction of the fibre (0°) from the PP manufacturing method are 10% and 54% greater than those of the VB and WL methods, respectively. The ultimate stresses of the PP along the fibre are 6% and 50% larger than VB and WL, respectively. The moduli of elasticity perpendicular to the direction of the fibre are between 5-6% of those parallel to the fibre direction from different manufacturing methods.

3.2 Hyperbaric chamber test results of the bare samples (Test plan 1)

The pressure response of the bare samples is plotted against the normalised change in the volume ($\Delta V/V_o$) (where ΔV is the volume of the water discharged from the pipe divided by V_o the initial volume of the pipe), for different D/t ratios in Fig. 7. Two distinctive pressures are identified in the response; (1) The initiation pressure (P_I) at which the collapse is initiated in the pipeline (the maximum value of the pressure inside the hyperbaric chamber before the propagation buckle occurred) , and is sensitive to the imperfection Δ_0 (shown on the figure), and (2) the propagation pressure (P_P) which is much smaller than the initiation pressure and is not imperfection sensitive (when the pressure dropped and stabilized). Previous researches [5, 40- 42] have shown that the initiation pressure is a combined elastic-plastic failure. The in-elastic expression (P_{CO}) suggested by Timoshenko [43] can be used to predict the collapse pressure of a pipe under uniform external pressure, based on its yield pressure (P_0), elastic critical buckling pressure (P_C), and imperfection parameter (φ):

$$P_{co} = \frac{1}{2}\left\{(P_0 + \varphi P_C) - [(P_0 + \varphi P_C)^2 - 4 P_0 P_C]^{0.5}\right\} \tag{3}$$

$$P_0 = \frac{2t\sigma_y}{D} \tag{4}$$

$$P_C = \frac{2E}{(1-\nu^2)}\left(\frac{t}{D}\right)^3 \tag{5}$$

$$\varphi = 1 + 3\Delta_0 \frac{D}{t} \tag{6}$$

The propagation pressure (P_P) can be predicted by the empirical expression suggested by Kyriakides and Lee [44] for stainless steel (SS304)

$$P_P = 20.69\sigma_y \left(\frac{t}{D}\right)^{2.362} \quad (7)$$

As can be seen in Fig. 7, the propagation pressures are very similar between different tests of each D/t. Using Eqs. 3 and 7, by substituting material properties from Table 1, and imperfections Δ_0, shown in Fig. 7, the collapse pressures and propagation pressures obtained from the experiments and the suggested equations are compared in Table 3. It can be seen from Table 3 that the propagation pressures predicted from Eq. 7 are similar to those obtained from the experiments with a maximum difference of 8%. However, the collapse pressures from Eq. 3 are 18% and 4% higher than those from the experiments for D/t of 28 and 40, respectively. Same conclusion was reported in [45] because, the Timoshenko's formula (Eq. 3) is known to give more accurate results in thin pipes (large D/t).

In Table 1, propagation pressures predicted from Eq.7 are represented based on 0.2% yield stress of the corresponding tensile test with the mentioned strain rate. The average values of P_P for D/t of 28 and 40 predicted from the fast rate are 2.75 MPa and 1.09 MPa, and from the slow rate are 2.62 MPa and 1.06 MPa, respectively. Therefore, using yield stress from the fast strain rate test in Eq.7 gives propagation pressures 4.9% and 2.8% greater than the slow rate for D/t of 28 and 40, respectively.

Images of the collapsed pipelines after the test, and during the test (using the buckle monitoring system) are also shown in Fig. 7. The failed pipelines removed from the pressure chamber showed a flat mode, whereas the pictures from inside the chamber and during the test, depict a dog-bone buckle mode. The flat buckle mode happens at higher pressures and when the buckle reaches the vicinity of the bulkhead. This is observed in the upsurge of the pressure towards the end of the pressure-volume responses in Fig. 7.

3.3 Parametric study on geometric parameters of CFRP buckle arrestors (Test plan 2)

A parametric study on effect of CFRP arrestor thickness (h), length (L), and fibre orientation ($\theta°$) using the PP manufacturing method and fine sanding surface finish, on the buckle propagation response of the pipeline with $D/t = 28.22$ is given here. The test configurations are shown in Fig. 5 and represented in Table 4. Pressure responses of the samples with CFRP arrestors (solid line) and corresponding bare samples (dotted line) are plotted in Figs. 8-10, in groups of 2 in each figure. The collapse starts at the location of the imposed imperfection (a distance $6D$ away from the bulkhead shown in Fig. 5). The pressure then drops, and the buckle

propagates towards the CFRP arrestors (A_i). The maximum pressure measured at the vicinity of each CFRP arrestor (the cross-over pressure) is denoted by P_{xi}. The increase in the pressure capacity due to the presence of the CFRP arrestor is shown as the ratio of the cross-over pressure (P_{xi}) divided by the propagation pressure of the bare sample (P_P). These ratios are represented in Table 4 for all tested configurations. As shown in Fig. 8a, a more congested positioning of the buckle arrestors (arrestor spacing smaller than 20D), does not increase the cross-over pressure. This was confirmed in the experimental tests of steel slip-on buckle arrestors [19], which suggests that a spacing of 20D between the buckle arrestors is sufficient. Comparison between results of Figs. 8a and 8b shows that, with $\theta = 90°$and $h/t = 1.0$, the cross-over ratio P_{xi}/P_P is always greater than 2.0, if L/D of 2.0 is maintained.

Maintaining $h/t = 1.0$ and $L/D = 2.0$, the CFRP arrestors were stacked in ±35° and ±55° biaxial orientation with respect to the longitudinal pipeline axis. The 35º angle mimics the steel armour orientation used in flexible subsea pipelines and risers [46]. As shown in Fig. 9, fractures were observed in all CFRP arrestors. No significant increase in the cross-over ratios compared to the propagation pressures of the bare samples was observed. This suggests that the optimum fibre orientation is $\theta = 90°$, which provides the maximum strength in the hoop direction.

Effect of h/t, maintaining $L/D = 1.0$ and $\theta = 90°$, on the cross-over pressure is shown in Fig. 10. A significant increase in P_{xi} is observed with $h/t = 2.0$, compared to $h/t = 1.0$. The close-up view of the CFRP arrestors shows that the largest cross-over pressure corresponds to the U-shape buckle mode observed in arrestors A_1 and A_2 in Fig. 10b. The same conclusion was reported in the confined buckle propagation modes investigated by Stepehn et al. [47] in single pipelines, Lee and Kyriakides [19] in slip-on buckle arrestors, and Karampour et al. [6] in pipe-in-pipe systems.

Time-history of pressure responses of all samples from the parametric study is shown in Fig. 11. The elapsed time from the initiation of the collapse, until the buckle reaches the arrestor A_i is marked on the curves. The time gap (Δt_d) between the onset of the buckle initiation (t=0) and the time at which the buckle crosses the respective arrestor, is denoted as the delay in buckle propagation. The largest delay was observed in the sample with $\theta = 90°$ and $h/t = 2.0$ (28E2PPF6, Fig. 10b). It took 31 seconds for the buckle to reach arrestor A1 and 51 seconds to reach arrestor A2. The second best in terms of delaying the buckle was the sample with $\theta = 90°$ and $L/D = 2.0$ (28D2PPF2, Fig. 8b), in which the buckle reached arrestor A1 in 11 seconds

and arrestor A2 in 33 seconds. In the bare sample (dashed line in Fig. 11) the buckle reached the opposite bulkhead in just 15 seconds.

A video (Video 1) of the buckle propagation of sample 28E2PPF6 inside the hyperbaric chamber is provided in the online version of the article. The buckle is initiated at t=5 s at the location of the imposed dent, in the far end of the chamber. The buckle propagates to A1, and is arrested until t=36 s. The buckle then crosses-over A1 and reaches A2 in about 0.24 seconds (equivalent to a speed of propagation equal to 0.22 m/s). The buckle is delayed between A1 and A2 (a clear length of 20D) for 20 seconds, at P_X/P_P = 3.

3.4 Effect of the manufacturing method (Test plan 3)

The parametric study (in test plan 2) revealed the superior performance of CFRP arrestors (manufactured with PP method) with h/t = 2 and θ = 90°. Therefore, in the manufacturing study (test plan 3), those parameters were adopted. Conservatively, a L/D=2 was adopted to ensure maximum cross-over pressure capacities are obtained. In test plan 3, only one single CFRP arrestor using VB and WL methods was installed at mid-length of the pipeline, to make certain that the capacity of the arrestor was not influenced by the end caps or adjacent arrestors. A schematic pressure vs. change of volume result from the hyperbaric chamber, showing the initiation, propagation and cross-over pressures is depicted in Fig 12. The pressure ratios are presented in Table 5. Result of the pipeline with the optimum CFRP arrestor configuration manufactured using the PP method (from test plan 2) is also included. Compared to P_X/P_P, the P_X/P_I ratio is a less reliable factor for comparison of performance of CFRPs. Because, although similar initial imperfections of almost identical magnitude were introduced to all pipes (Table 5), the initiation pressures depict some differences. The reason is associated with the anisotropy in yielding introduced during the manufacturing process of seamless tubes, which in turn can affect the initiation pressure [48].

Hyperbaric chamber results showed that all tested pipelines deformed in a flatten buckle mode, the buckle penetrated through the CFRP arrestor in a U-shape buckle mode. No fractures were observed in the CFRP arrestors. In all samples, regardless of the manufacturing method and surface preparation, P_X/P_P larger than 3 were observed at either D/t. However, the results in Table 5 clearly show that the cross-over pressure (P_X) is affected by the manufacturing technique and the surface preparation method. Despite lower moduli of elasticity of WL samples compared to others (Table 2), no significant change in P_X/P_P from different manufacturing methods are observed, this means that the P_X/P_P is not significantly affected by

the moduli of elasticity of buckle arrestor . On the other hand, the fine sanding consistently enhances the cross-over ratio P_X/P_P, with an average of 20% increase compared to the coarse sanding.

Time-history of pressure responses for each D/t is shown in Fig. 13. The figure shows the elapsed time from the initiation of the collapse until the buckle reaches the CFRP arrestor. The buckle arrestor delay times (Δt_d) are given in Table 5. The largest Δt_d corresponds to the WL manufacturing method with fine sanding. The VB method comes second in terms of delaying the buckle.

3.5 Efficiency of CFRP buckle arrestors (comparison with slip-on and integral arrestors)

Gong and Li [49] performed a parametric study to measure the cross-over pressure (P_X/P_P) in integral buckle arrestor based on the geometric parameters, D/t and h/t. They proposed the following empirical equation for pipelines with $15 < D/t < 35$

$$\frac{P_X}{P_P} = 1 + 1.086\left(\frac{t}{D}\right)^{0.46}\left(\frac{h}{t}\right)^{3.05} \tag{8}$$

By using Eq. 8 and the parameters in Table 5, the cross-over ratio P_X/P_P of 2.94 and 2.65 are calculated for pipes with $D/t \approx 28$ and 40, respectively. All of the experimental P_X/P_P in Table 5 for current CFRP arrestors are larger than those predicted by Eq. 8. Moreover, Gong and Li [49] found that in integral arrestors, the cross-over ratio P_X/P_P decreases with the increase in D/t. However, current results show that in CFRP arrestors the P_X/P_P is not affected by the D/t of the pipeline.

The arresting efficiency (η_{CFRP}) of the CFRP arrestors are listed in Table 6. The propagation pressures (P_P) and cross-over pressures (P_X), are taken from the experimental results. The collapse pressure (P_{CO}) of each sample is calculated using the Timoshenko's formula (Eq. 3). Then, these pressures are used to find the CFRP arrestor efficiency (η_{CFRP}) in accordance with Eq. 1.

It can be seen from Table 6 that the pipeline with D/t of 28 yields higher efficiencies compared to the pipeline with D/t of 40, regardless of the manufacturing and surface preparation methods.

Efficiencies almost equal to 1.0 are observed in the pipeline with D/t of 28 and using the WL method with fine sanding. Lowest efficiencies are observed in samples manufactured with the VB method and coarse sanding. Using mechanical properties obtained from coupon tests performed at faster strain rates, lower efficiencies are calculated. On average, differences between efficiencies at fast and slow rates for $D/t \approx 28$ and 40, are 4.7% and 1.2%, respectively.

Kyriakides and Lee [19, 22] performed hyperbaric tests on 22 stainless steel pipelines with D/t between 14 and 94 and slip-on buckle arrestors of various geometric configurations. Based on the experimental results, they proposed empirical expressions and upper/lower bounds for efficiency of slip-on arrestors at different D/t. Fig.14 shows efficiencies of the CFRP arrestors from the current study compared with the lower and upper bounds for slip-on arrestors from [19]. As shown in Fig. 14, at $D/t \approx 28$ the slip-on arrestor efficiencies range between 0.68 to 0.81. However, except 2 test results, all measured CFRP efficiencies are larger than the predicted upper bound for slip-on arrestors. At $D/t \approx 40$, the efficiencies of CFRP arrestors drop and are closer to the predicted lower bound for slip-on arrestors. The CFRP efficiencies with coarse sanding in WL and VB methods are below the lower bound of slip-on arrestors at $D/t \approx 40$. It should be noted that to obtain the lower bound efficiency in slip-on arrestors in Fig. 14, $h \geq 2.5t$ should be maintained [19]; however, the CFRP arrestors use $h=2t$.

Kyriakides and Park [18, 50] performed comprehensive experimental and numerical studies on the design of the integral buckle arrestors. They found a minimum required thickness (h_{cm}) for the integral buckle arrestors, at which the cross-over pressure (P_X) becomes equal to the collapse pressure of the pipe (P_{CO}), i.e. efficiency of 1. By comparing the results from the current study to the predictions in [18, 50], $h_{cm} = 3.5t$ and $4.6t$ are required (for $D/t \approx 28$ and 40, respectively) using integral arrestors to achieve similar efficiencies to CFRP arrestors with $h=2t$ as listed in Table 6.

4. Conclusions

Buckling responses of steel pipelines with CFRP buckle arrestors were experimentally investigated using hyperbaric chamber tests. The CFRP buckle arrestors were fabricated and installed on steel pipelines with $D/t \approx 28$ and $D/t \approx 40$ using three manufacturing techniques: (1) vacuum bagging (VB), (2) wet lay-up (WL), and (3) prepreg (PP) methods. Two different surface preparation methods were tested, (a) fine sanding, and (b) coarse sanding. Mechanical properties of the steel pipes and CFRP sheets were obtained from standard coupon tests at

different strain rates. The hyperbaric chamber tests were performed in 3 test plans; (1) bare samples, (2) parametric study on effect of thickness (h), length (L), and orientation ($\theta°$) of the CFRP arrestor, on its cross-over capacity (only PP method and with $D/t \approx 28$), and (3) the effect of the manufacturing technique and D/t ratio.

The following significant outcomes were found from the current work:

- The CFRP arrestors build large cross-over pressures and significantly delay the buckle propagation in the pipeline.
- The optimum fibre orientation of the CFRP arrestor is $\theta = 90°$, which provides the maximum stiffness in the hoop direction.
- The optimum manufacturing technique is the WL method with fine sanding, which provides the maximum buckle capacity and longest delay of the buckle propagation.
- The cross-over pressure (P_X) is affected by the manufacturing technique and the surface preparation method. However, by adopting $\theta = 90°$, $h/t = 1.0$, and $L/D = 2.0$ a minimum cross-over ratio (P_{xi}/P_P) equal to 3 can be achieved, regardless of the D/t ratio of the pipeline or the manufacturing method.
- The efficiency of a CFRP arrestor installed on a pipeline with D/t =28 (used in deep waters) is higher than the predicted upper bound efficiency of a slip-on arrestor [19] with similar parameters.
- To achieve similar efficiencies, the integral buckle arrestors need to be 1.75 and 2.3 times thicker than the proposed CFRP arrestors, for D/t=28 and 40, respectively.
- Unlike slip-on and integral buckle arrestors, the normalised cross-over capacity (P_{xi}/P_P) of a CFRP arrestor is independent of the D/t ratio of the pipeline.

Current results showed that the proposed CFRP arrestors can be an appropriate alternative to the existing slip-on and integral buckle arrestors, however, further research is required to investigate the conductivity issue for CFRP.

References

[1] Zhang, Y.M., Tan, T.K., Xiao, Z.M., Zhang, W.G. and Ariffin, M.Z., 2016. Failure assessment on offshore girth welded pipelines due to corrosion defects. Fatigue & Fracture of Engineering Materials & Structures, 39(4), 453-466.

[2] Gamboa, E., Linton, V. and Law, M., 2008. Fatigue of stress corrosion cracks in X65 pipeline steels. International journal of fatigue, 30(5), 850-860.

[3] Zhang, Y.M., Ariffin, M.Z., Xiao, Z.M., Zhang, W.G. and Huang, Z.H., 2015. Nonlinear elastic–plastic stress investigation for two interacting 3-D cracks in offshore pipelines. Fatigue & Fracture of Engineering Materials & Structures, 38(5), 540-550.

[4] Zhang, Y.M., Fan, M., Xiao, Z.M. and Zhang, W.G., 2016. Fatigue analysis on offshore pipelines with embedded cracks. Ocean Engineering, 117, pp.45-56.

[5] Albermani F, Khalilpasha H, Karampour H. Propagation buckling in deep sub-sea pipelines. Engineering Structures 2011;33:2547-2553.

[6] Karampour H, Alrsai M, Albermani F, Guan H, Jeng DS. Propagation buckling in subsea pipe-in-pipe systems. Journal of Engineering Mechanics 2017;143(9):04017113.

[7] Alrsai M, Karampour H, Albermani F. Numerical study and parametric analysis of the propagation buckling behaviour of subsea pipe-in-pipe systems. Thin-Walled Structures 2018;125:119-128.

[8] He T, Duan M, An C. Prediction of the collapse pressure for thick-walled pipes under external pressure. Applied Ocean Research 2014;47:199-203.

[9] Alrsai M, Karampour H, Albermani F. On collapse of the inner pipe of a pipe-in-pipe system under external pressure. Engineering Structures 2018;172:614-628.

[10] Yan ST, Shen XL, Jin ZJ, Ye H. On elastic-plastic collapse of subsea pipelines under external hydrostatic pressure and denting force. Applied Ocean Research. 2016;58:305-21.

[11] Karampour H, Albermani F, Veidt M. Buckle interaction in deep subsea pipelines. Thin-Walled Structures 2013;72:113-120.

[12] Karampour H, Albermani F. Buckle interaction in textured deep subsea pipelines. Ships and Offshore Structures 2016;11(6):625-635.

[13] Karampour H, Albermani F. Experimental and numerical investigations of buckle interaction in subsea pipelines. Engineering Structures 2014;66:81-88.

[14] Karampour H, Albermani F, Major P. Interaction between lateral buckling and propagation buckling in textured deep subsea pipelines. In ASME 2015 34th International Conference on Ocean, Offshore and Arctic Engineering.ASME 2015.

[15] Karampour H, Effect of proximity of imperfections on buckle interaction in deep subsea pipelines. Marine Structures 2018;59:444-457.

[16] DNV G. Standard DNVGL-ST-F101 Submarine pipeline systems, 2017.

[17] Netto TA, Estefen SF. Buckle arrestors for deepwater pipelines. Marine structures. 1996;9(9):873-83.

[18] Kyriakides S, Park TD, Netto TA. On the design of integral buckle arrestors for offshore pipelines. Applied ocean research 1998;20(1-2):95-104.

[19] Lee LH, Kyriakides S. On the arresting efficiency of slip-on buckle arrestors for offshore pipelines. International journal of mechanical sciences 2004;46(7):1035-55.

[20] Kyriakides S, Babcock CD. "The Spiral Arrester"—A New Buckle Arrestor Design for Offshore Pipelines. J. Energy Resour. Technol.1982:73-77.

[21] Kyriakides S, Babcock CD. On the dynamics and the arrest of the propagating buckle in offshore pipelines. In Offshore Technology Conference 1979:1035-1045.

[22] Kyriakides S. Efficiency limits for slip-on type buckle arrestors for offshore pipelines. Journal of engineering mechanics. 2002;128(1):102-111.

[23] Yu JX, Duan JH, Sun ZZ, Yu Y, Wu MN. The cross-over mechanisms of integral buckle arrestors for offshore pipelines. Applied Ocean Research. 2017;67:236-47.

[24] Wonderly C, Grenestedt J, Fernlund G, Cêpus E. Comparison of mechanical properties of glass fibre/vinyl ester and carbon fibre/vinyl ester composites. Composites: Part B: Eng. 2005;36:417–26

[25] Keller MW, Jellison BD, Ellison T. Moisture effects on the thermal and creep performance of carbon fiber/epoxy composites for structural pipeline repair. Composites Part B: Eng. 2013;45:1173–80.

[26] Goertzen WK, Kessler MR. Dynamic mechanical analysis of carbon/epoxy composites. Composites: Part B: Eng. 2007;38:1–9.

[27] Sen R, Mullins G. Application of FRP composites for underwater piles repair.Composites: Part B: Eng. 2007;38:751–8.

[28] Shamsuddoha M, Islam MM, Aravinthan T, Manalo A, Lau KT. Effectiveness of using fibre-reinforced polymer composites for underwater steel pipeline repairs. Composite Structures. 2013;100:40-54.

[29] Duell JM, Wilson JM, Kessler MR. Analysis of a carbon composite overwrap pipeline repair system. International Journal of Pressure Vessels and Piping. 2008;85(11):782-8.

[30] Seica MV, Packer JA. FRP materials for the rehabilitation of tubular steel structures, for underwater applications. Composite Structures. 2007;80(3):440-50.

[31] Lukács J, Nagy G, Török I, Égert J, Pere B. Experimental and numerical investigations of external reinforced damaged pipelines. Procedia Engineering. 2010;2(1):1191-200.

[32] Lukács J, Nagy G, Török I. The role of the external and internal reinforcing on the structural integrity of damaged steel pipelines. Procedia Engineering. 2011;10:2514-9.

[33] Smith SN, Clough T. Deepwater pipeline installation by reel-lay method. In Offshore Technology Conference 2010 Jan 1. Offshore Technology Conference.

[34] Olso E, Kyriakides S. Internal ring buckle arrestors for pipe-in-pipe systems. International journal of non-linear mechanics. 2003;38(2):267-84.

[35] Alrsai M, Karampour H. Propagation buckling of pipe-in-pipe systems, an experimental study. InThe Twelfth ISOPE Pacific/Asia Offshore Mechanics Symposium 2016 Oct 4. International Society of Offshore and Polar Engineers.

[36] Karampour H, Alrsai M, Hall W. Efficiency of Carbon Fibre Buckle Arrestors for Subsea Pipelines. In ASME 2019 38th International Conference on Ocean, Offshore and Arctic Engineering. American Society of Mechanical Engineers Digital Collection.

[37] Australian Standard. Metallic materials-tensile testing at ambient temperature. AS 1391-2007, Australia. 2007.

[38] ASTM S. D3039/D3039M-08. Standard test method for tensile properties of polymer matrix composite materials. 2008.

[39] A.C.G. Ltd. in ACG VTM 260 Series Product Description. 2018.

[40] Chater E, Hutchinson JW. On the propagation of bulges and buckles. Journal of applied mechanics. 1984;51(2):269-77.

[41] Kyriakides S, Babcock CD, Elyada D. Initiation of propagating buckles from local pipeline damages. 1984; 79-87.

[42] Li Z, An C, Duan M. An analytical approach for elastic and non-elastic buckling of pipes under external/internal pressures. Ocean Engineering. 2019;187:106160.

[43] Timoshenko SP, Gere JM. Theory of elastic stability. McGrawHill-Kogakusha Ltd, Tokyo; 1961.

[44] Kyriakides S, Lee LH. Buckle propagation in confined steel tubes. International journal of mechanical sciences. 2005;47(4-5):603-20.

[45] Kyriakides S, Corona E. Mechanics of offshore pipelines: volume 1 buckling and collapse. Elsevier; 2007 Jul 26.

[46] Sævik S, Li H. Shear interaction and transverse buckling of tensile armours in flexible pipes. In ASME 2013 32nd international conference on ocean, offshore and arctic engineering 2013 Jun 9. American Society of Mechanical Engineers Digital Collection.

[47] Stephan P, Love C, Albermani F, Karampour H. Experimental study on confined buckle propagation. Adv. Steel Constr 2016;12(1):44-54.

[48] Kyriakides S, Yeh MK. Plastic anisotropy in drawn metal tubes. Journal of Engineering for Industry. 1988;110(3):303-7.

[49] Gong S, Li G. On the prediction of arresting efficiency of integral buckle arrestors for deepwater pipelines. International Journal of Steel Structures. 2017;17(4):1443-58.

[50] Park TD, Kyriakides S. On the performance of integral buckle arrestors for offshore pipelines. International Journal of Mechanical Sciences. 1997;39(6):643-69.

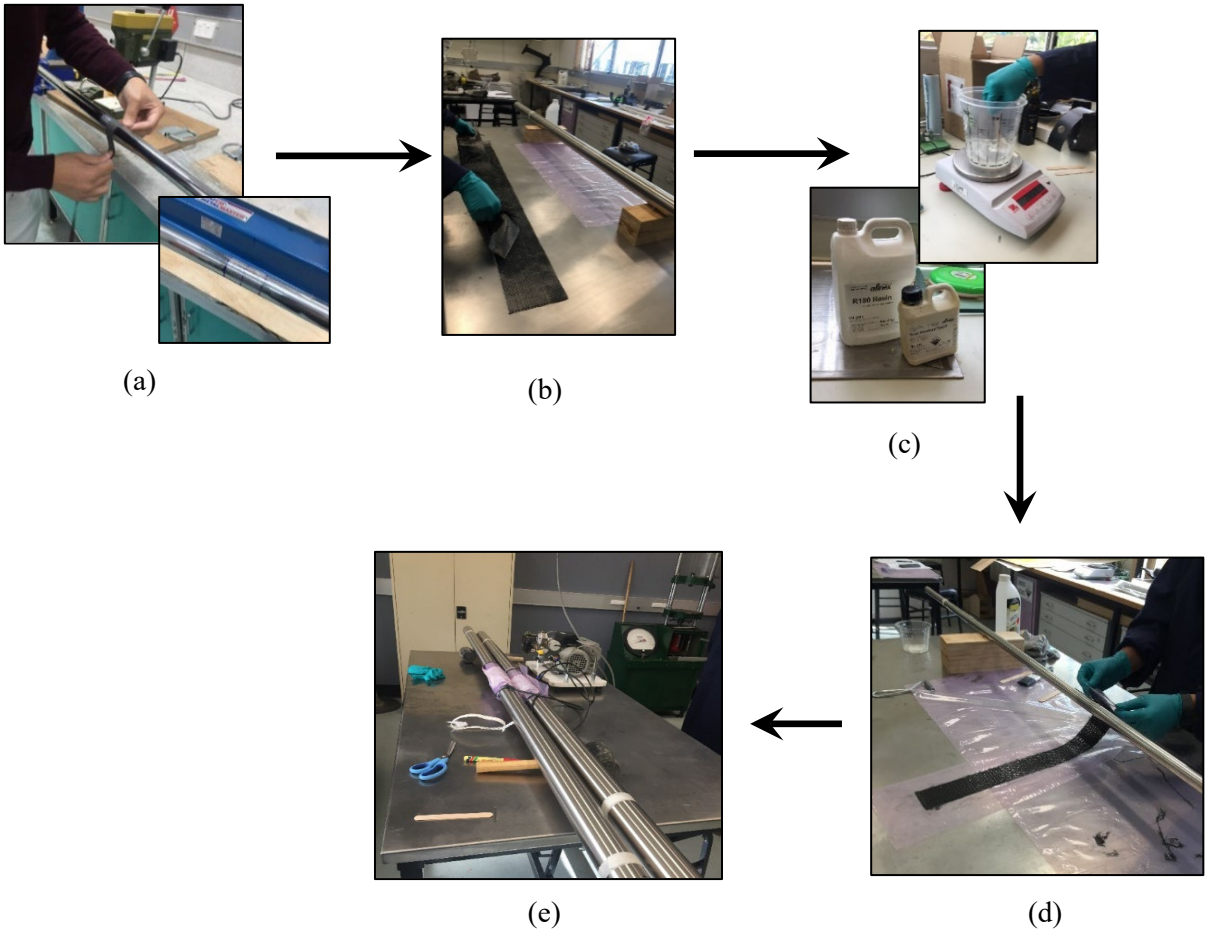

Fig.1. The manufacturing process for the vacuum bagging (VB) method; (a) Sample preparations; includes Surface sanding (course and fine) and Sample marking; (b) Cut CFRP layers in the required width; (c) Mix the required amount of the resin and hardener; (d) Wrap the CFRP layers in hoop direction; and (e) Place the vacuum over the samples for curing (24 hours @ room temperature).

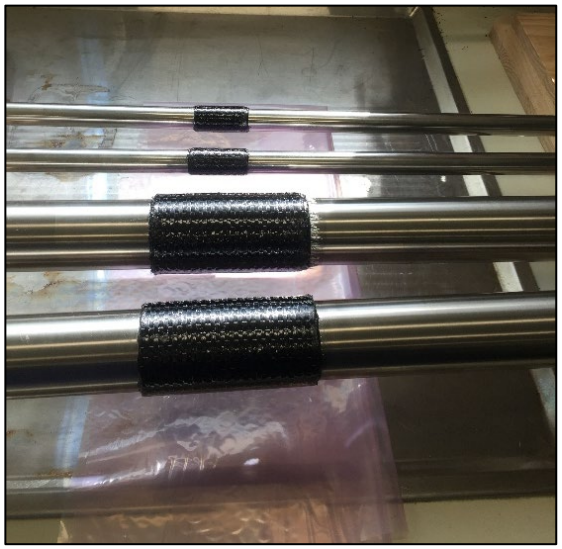

Fig.2. Curing process in wet lay-up (WL) method.

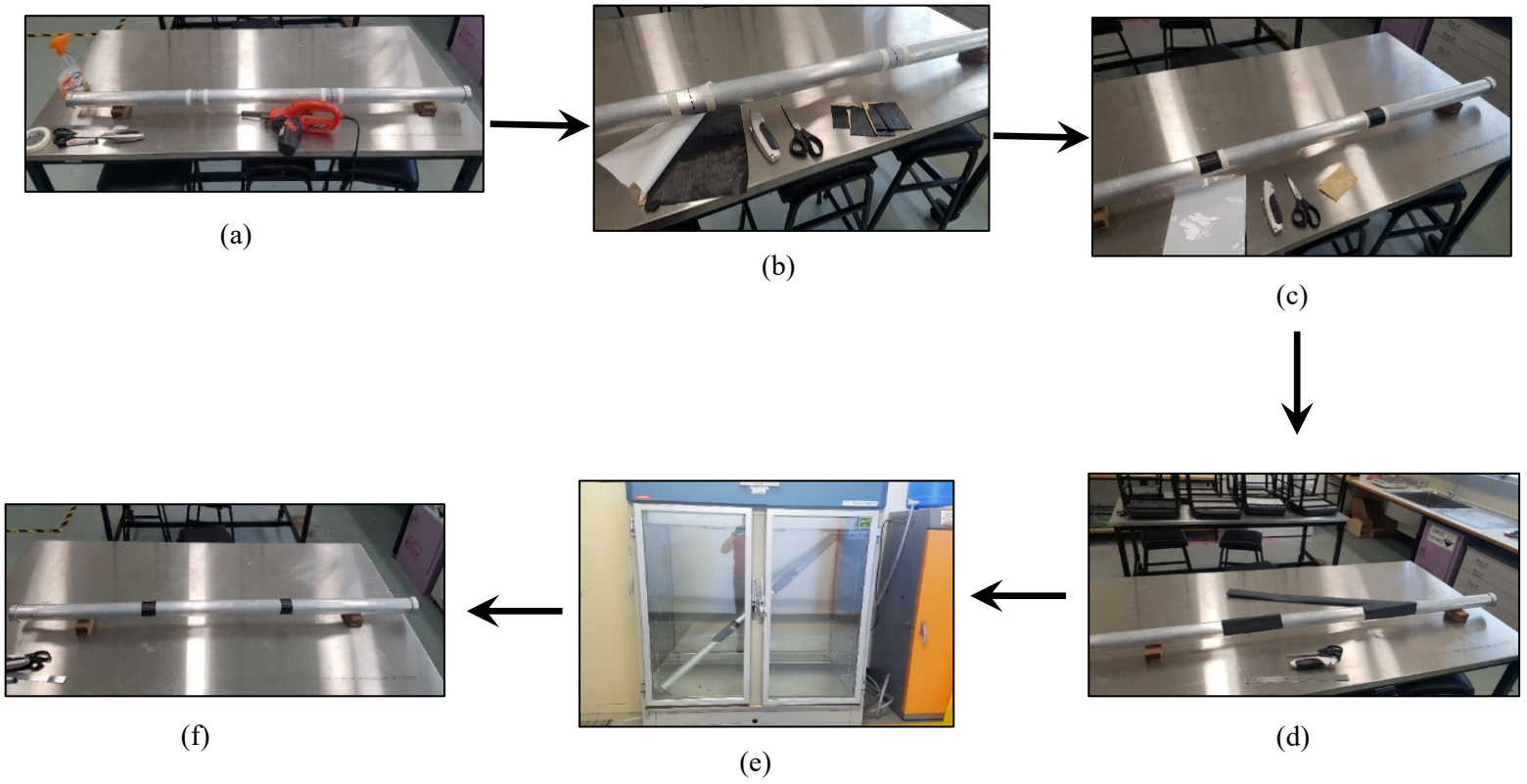

Fig.3. The manufacturing process in the pre-preg (PP) method; (a) Sample preparations; includes Surface sanding and Sample marking; (b) Cut CFRP layers in required dimension and orientation; (c) Wrap the required number of CFRP layers; (d) Slide the shrink tube over the CFRP to provide consolidation pressure; (e) Insert the sample into the oven for curing (2 hours @ 120°C); (f) Ready for test.

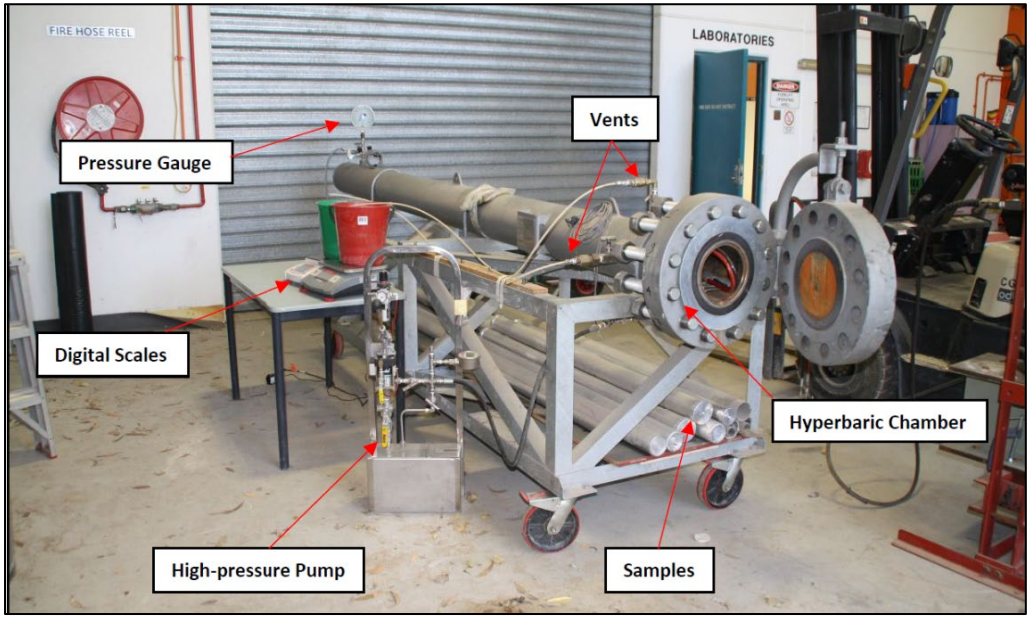

(a)

(b)

Fig. 4. Experimental setup (a) hyperbaric chamber, high-pressure pump, scales, pressure gauge, and vents; (b) the buckle monitoring system.

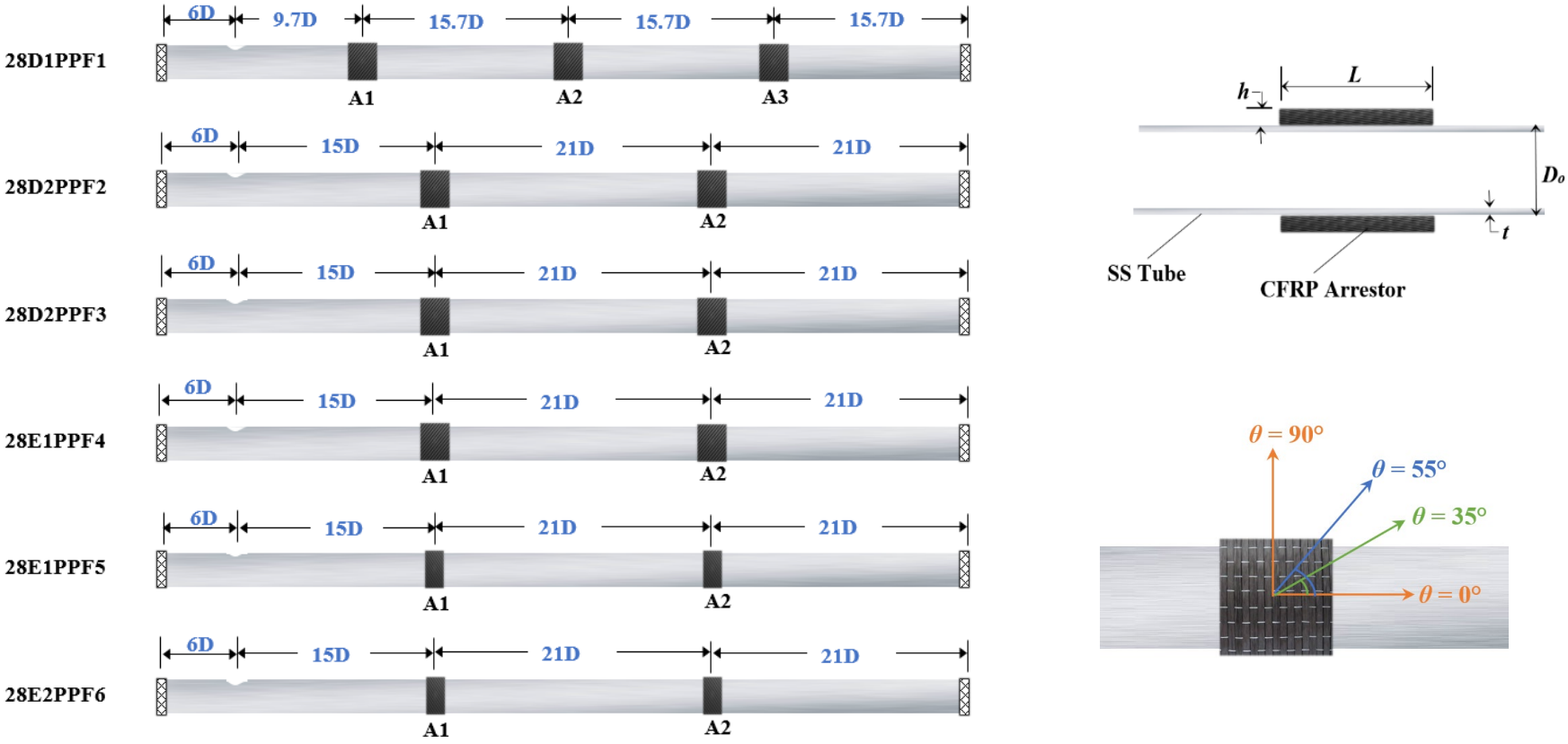

Fig. 5. The Stainless-steel tube samples (D=24.5mm and t=0.9mm) with different CFRP arrestor configurations (Test plan 2).

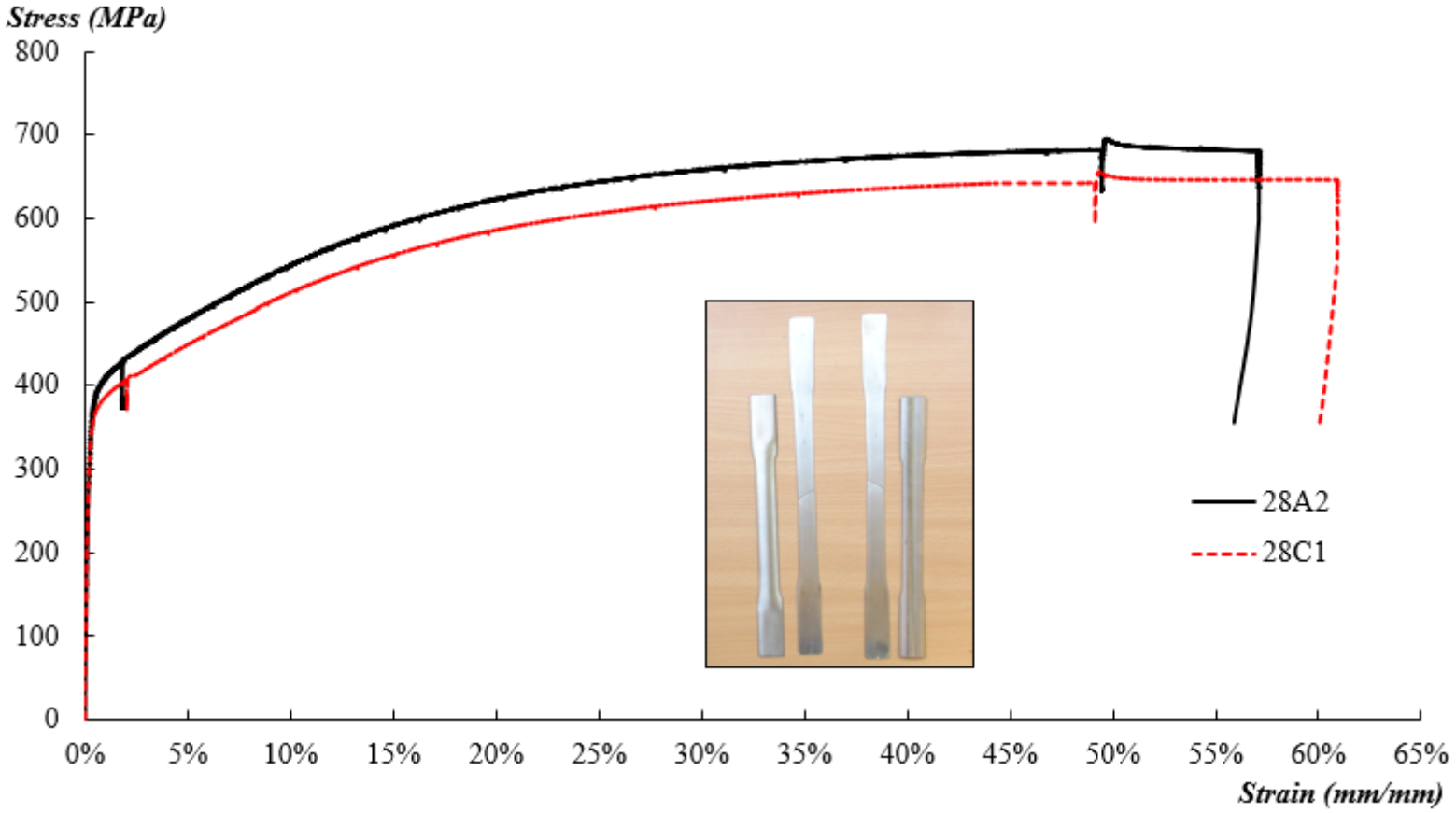

Fig. 6. Typical coupon results, showing stress-strain curves at strain rates of 0.333 $\times 10^{-3}$ (s^{-1}) and 2.667 $\times 10^{-3}$ (s^{-1}) for samples 28C1 and 28A2, respectively (refer to Table 1).

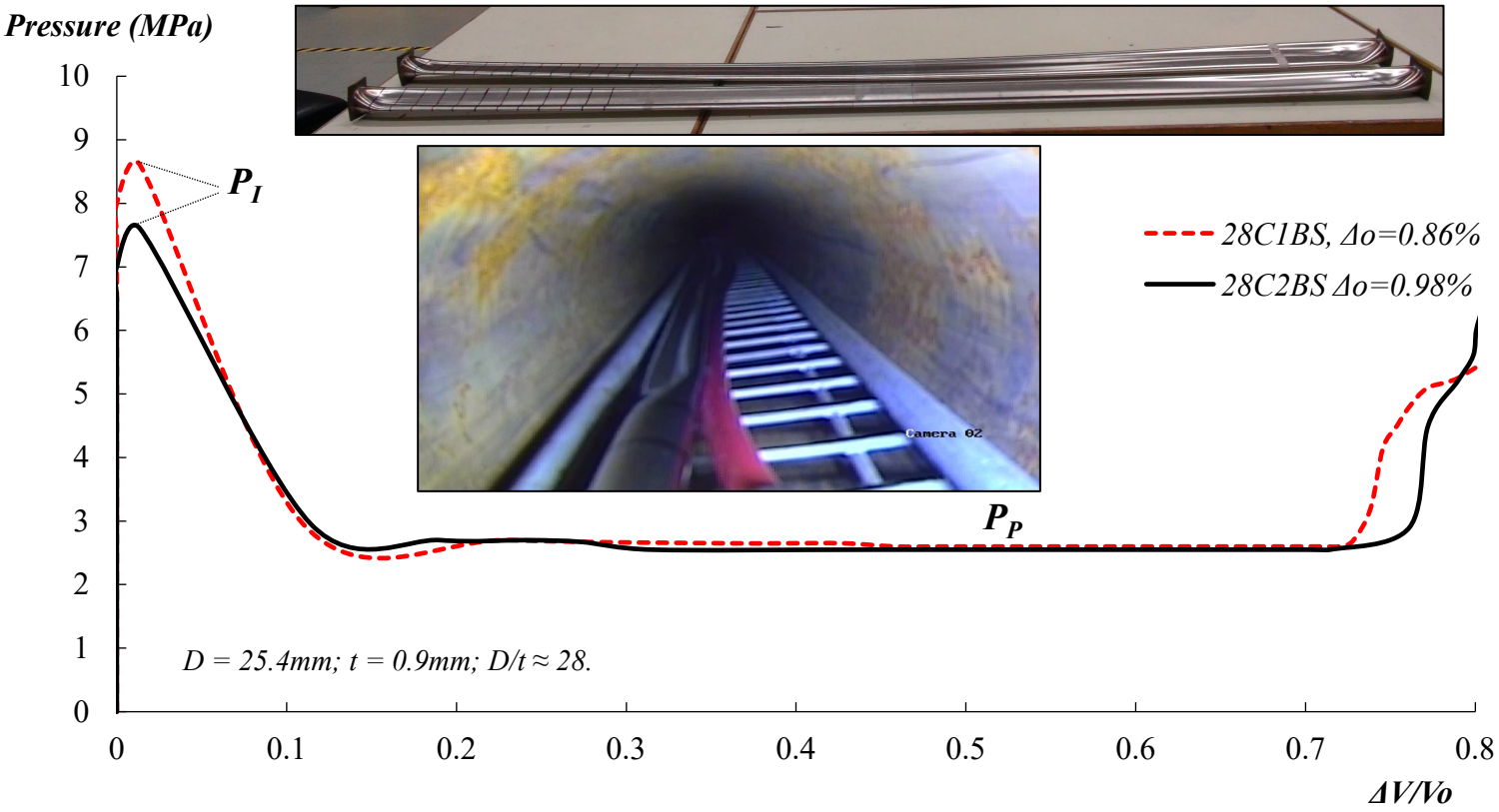
Pressure (MPa)
10
9
8
7
6
5
4
3
2
1
0
P_I
P_P
28C1BS, Δo=0.86%
28C2BS Δo=0.98%
D = 25.4mm; t = 0.9mm; D/t ≈ 28.
0
0.1
0.2
0.3
0.4
0.5
0.6
0.7
0.8
ΔV/Vo

(a)

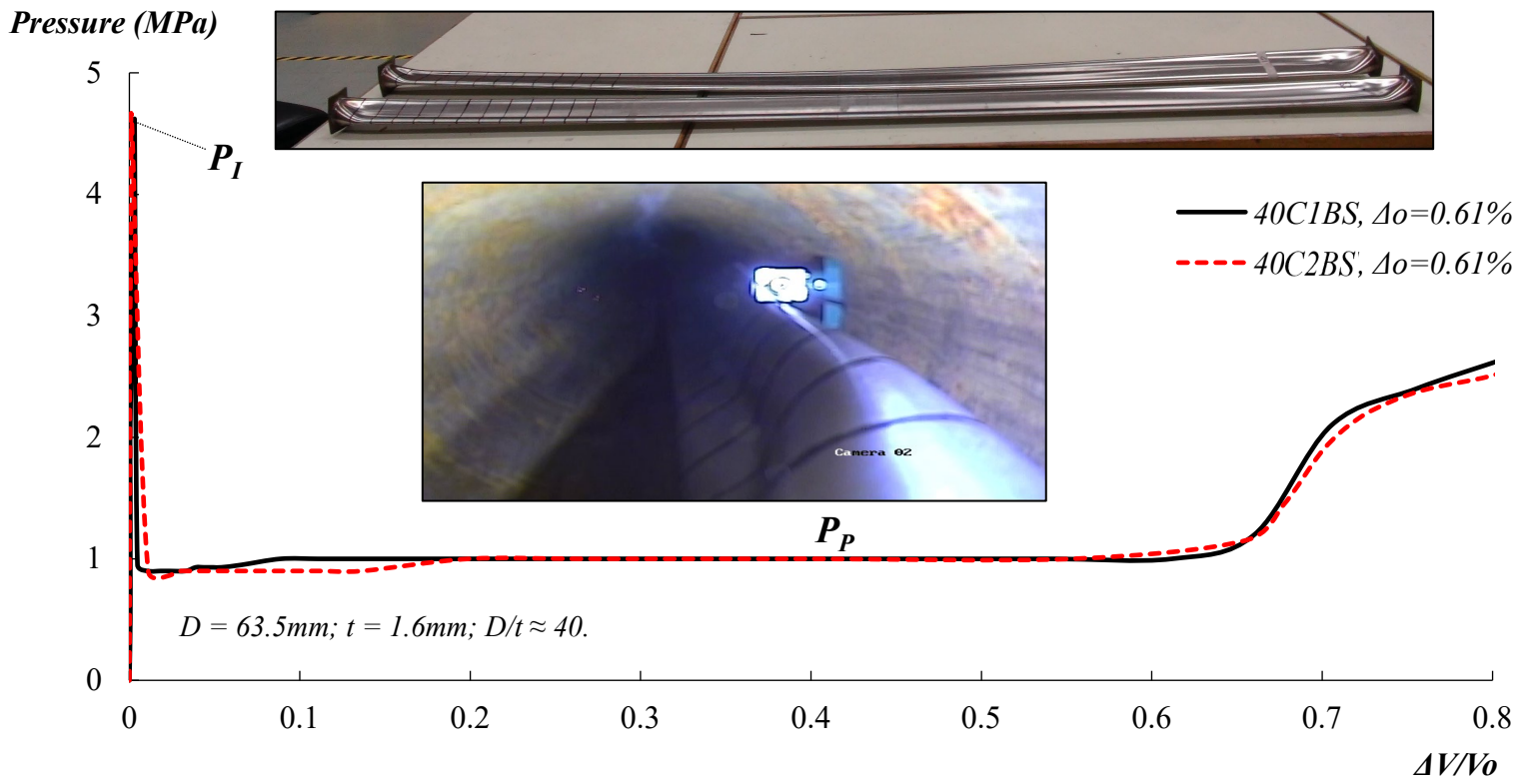

(b)

Fig. 7. Pressure-volume response from the hyperbaric chamber tests of the bare samples (a) $D/t \approx 28$, showing a snapshot from high-pressure camera of the buckled tube, (b) $D/t \approx 40$, showing a snapshot from high-pressure camera showing of buckled tube. Failed samples are removed from the chamber also shown.

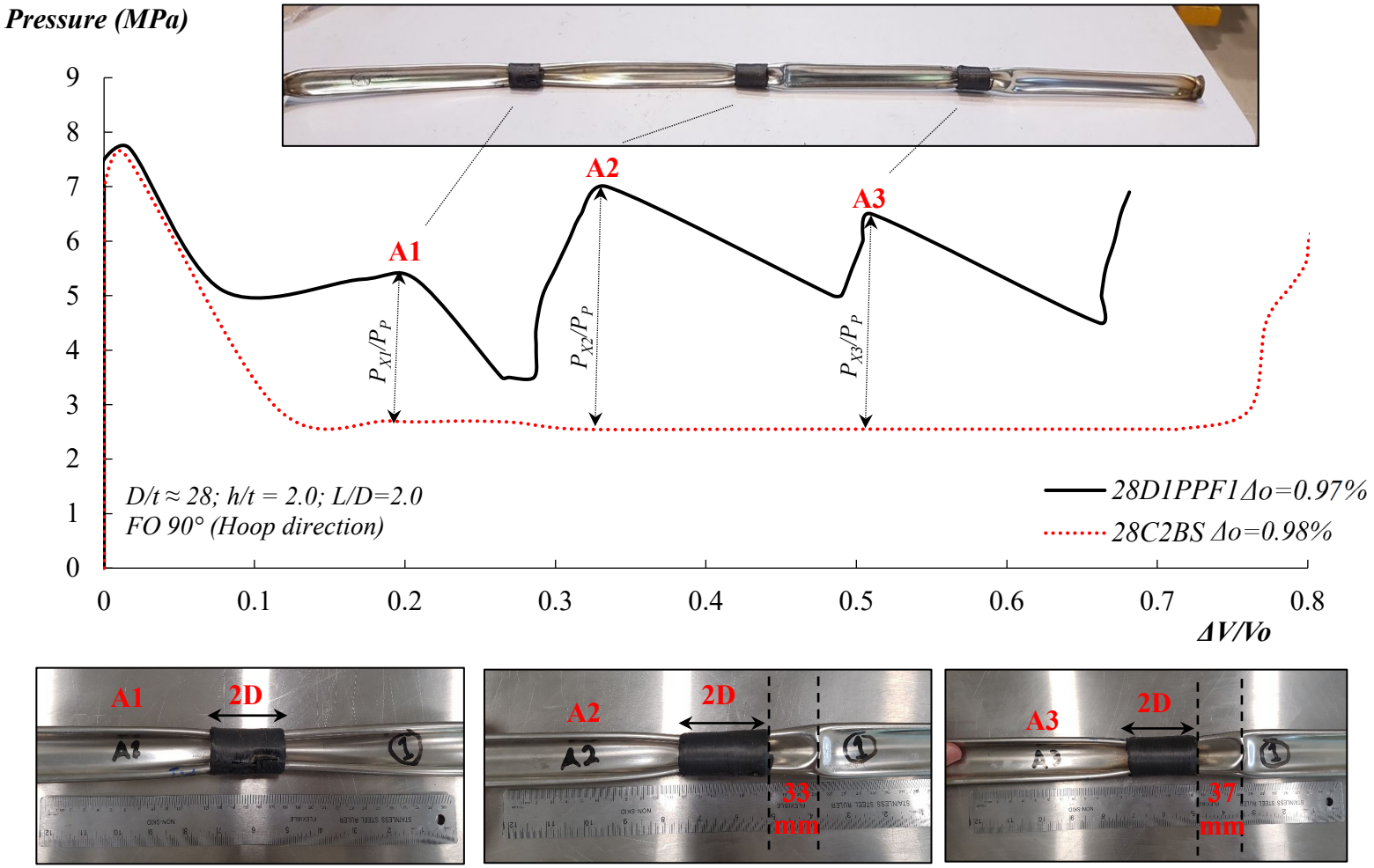
Pressure (MPa)
9
8
7
6
5
4
3
2
1
0
A1
A2
A3
P_{X1}/P_P
P_{X2}/P_P
P_{X3}/P_P
D/t ≈ 28; h/t = 2.0; L/D=2.0
FO 90° (Hoop direction)
28D1PPF1Δo=0.97%
28C2BS Δo=0.98%
0
0.1
0.2
0.3
0.4
0.5
0.6
0.7
0.8
ΔV/Vo
A1
2D
A2
2D
33
mm
A3
2D
37
mm

(a)

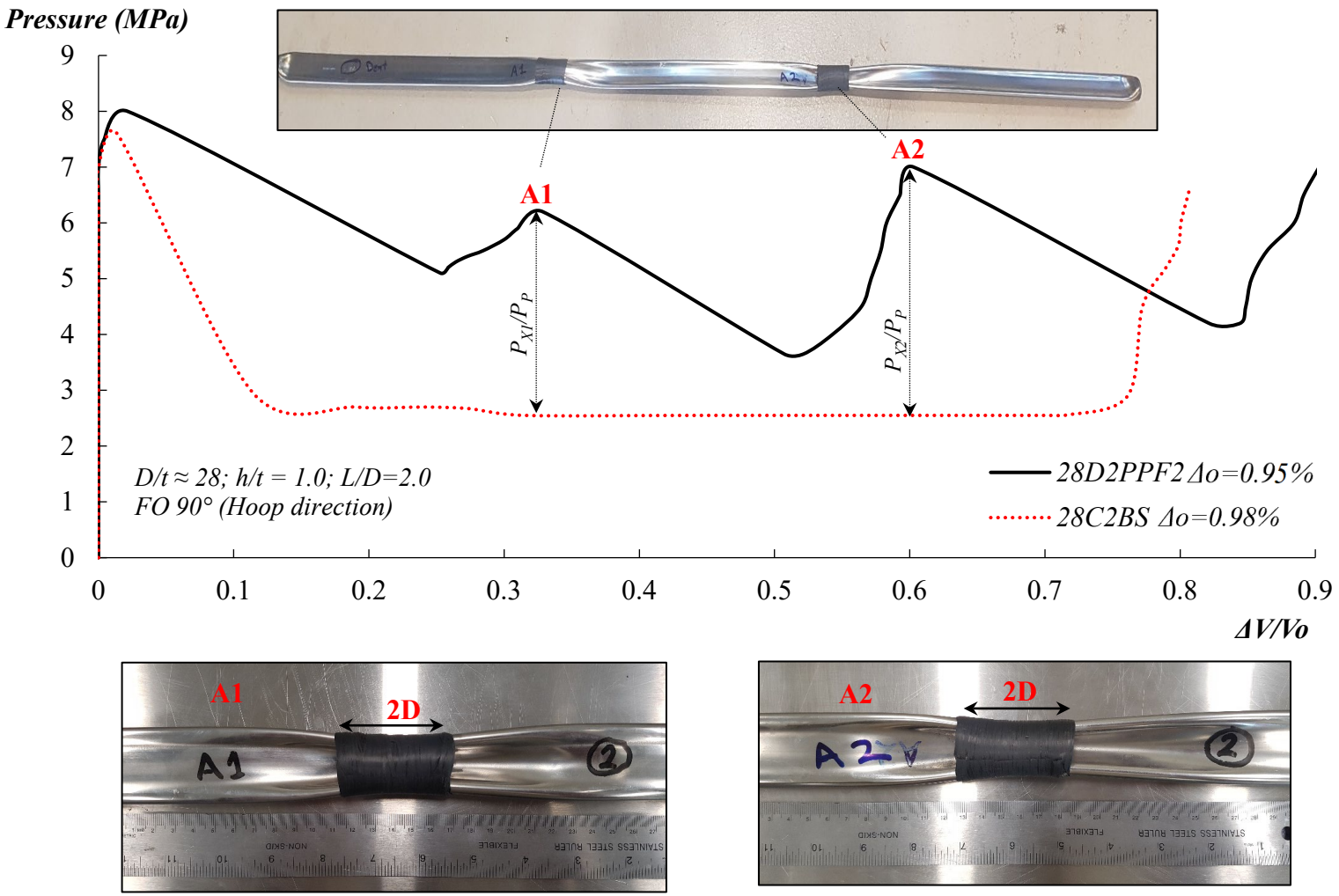

(b)

Fig. 8. Pressure responses of; (a) sample 28D1PPF1, and (b) sample 28D2PPF2.

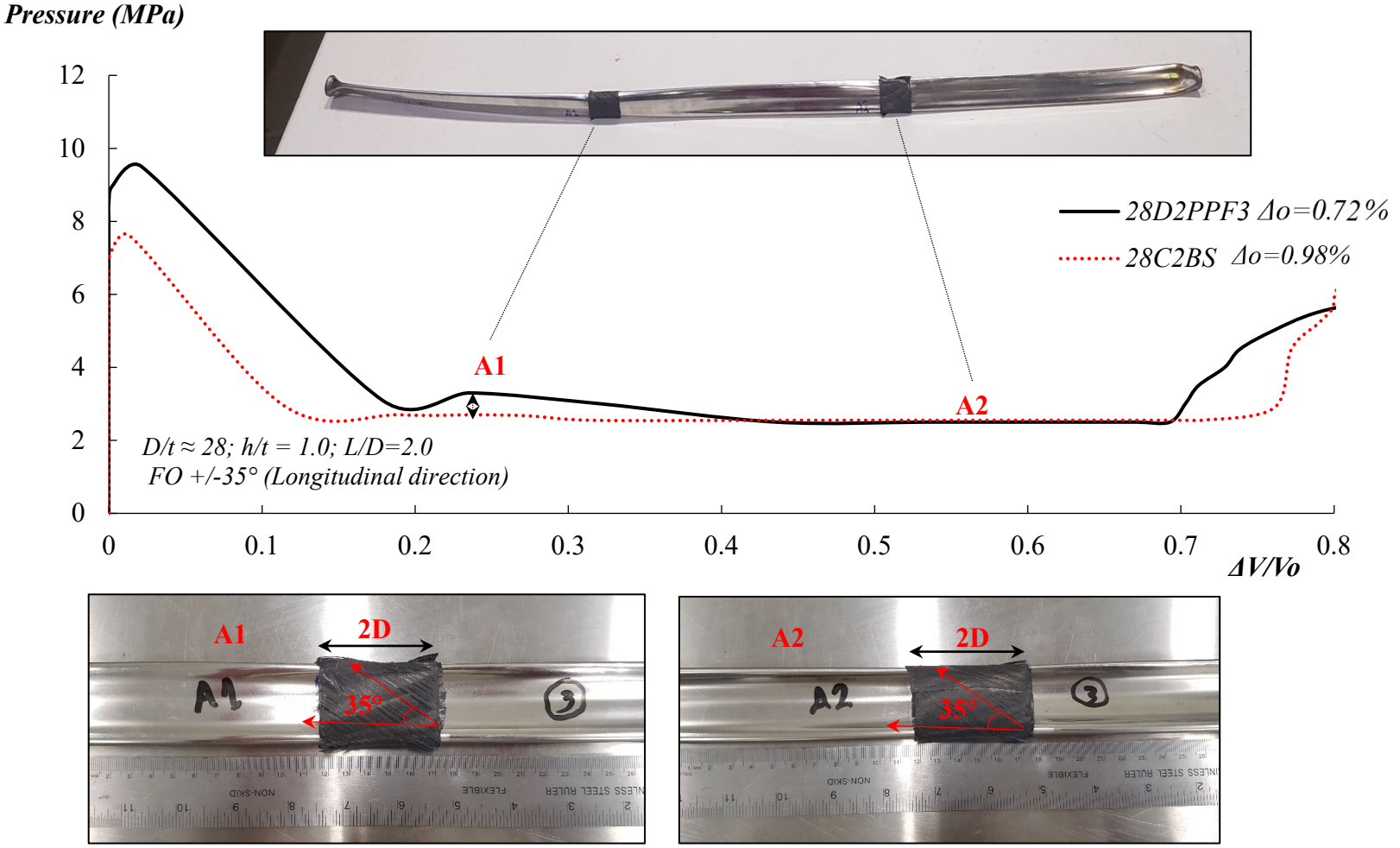
Pressure (MPa)
12
10
8
6
4
2
0
0
0.1
0.2
0.3
0.4
0.5
0.6
0.7
0.8
ΔV/Vo
28D2PPF3 Δo=0.72%
28C2BS Δo=0.98%
A1
A2
D/t ≈ 28; h/t = 1.0; L/D=2.0
FO +/-35° (Longitudinal direction)
A1
2D
35°
A2
2D
35°

(a)

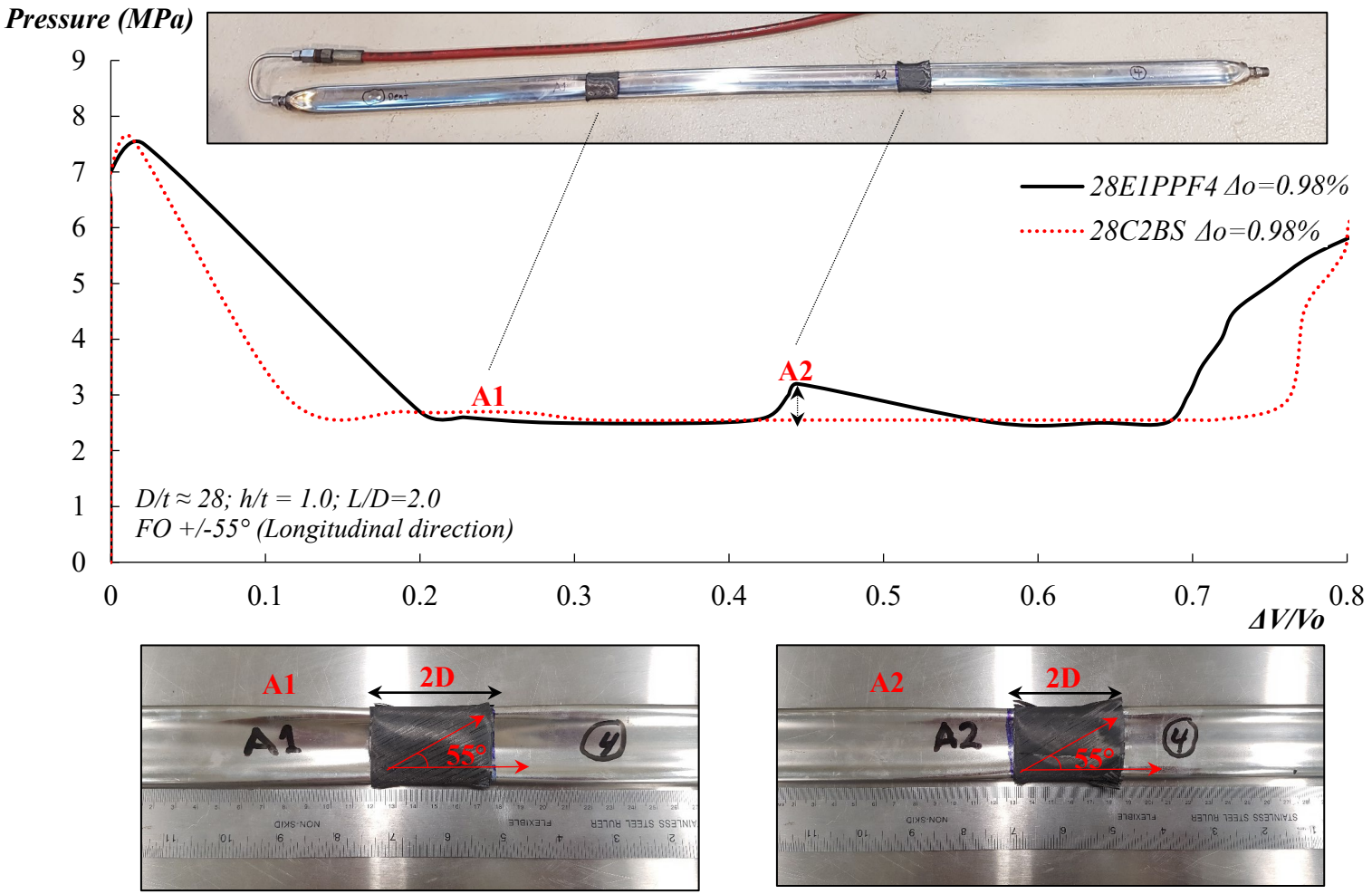

(b)

Fig.9. Pressure responses of; (a) sample 28D2PPF3, and (b) sample 28E1PPF4.

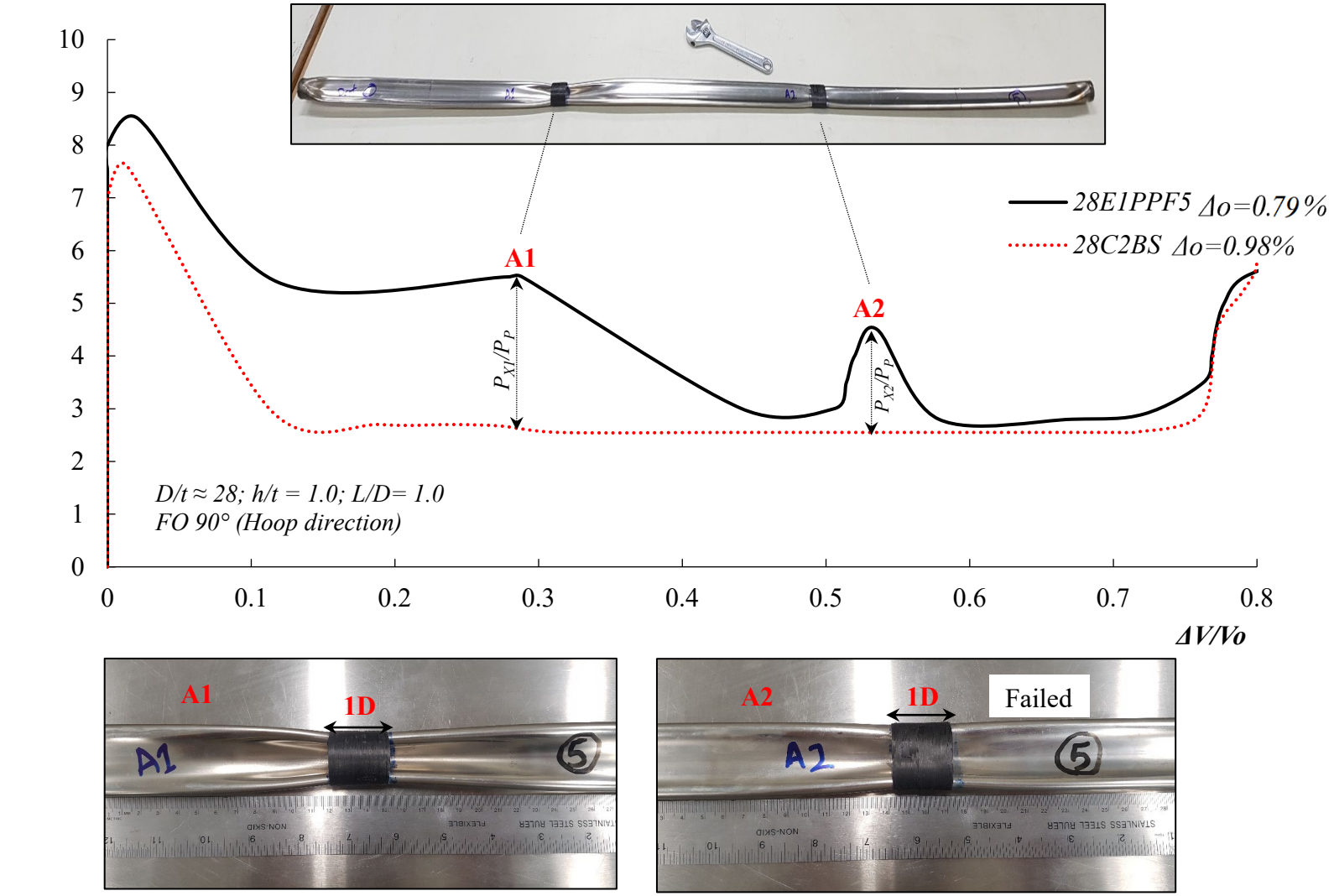
Pressure (MPa)
10
9
8
7
6
5
4
3
2
1
0
0
0.1
0.2
0.3
0.4
0.5
0.6
0.7
0.8
ΔV/Vo
28E1PPF5 Δo=0.79%
28C2BS Δo=0.98%
A1
A2
P_{X1}/P_P
P_{X2}/P_P
D/t ≈ 28; h/t = 1.0; L/D= 1.0
FO 90° (Hoop direction)
A1
1D
A1
5
A2
1D
Failed
A2
5

(a)

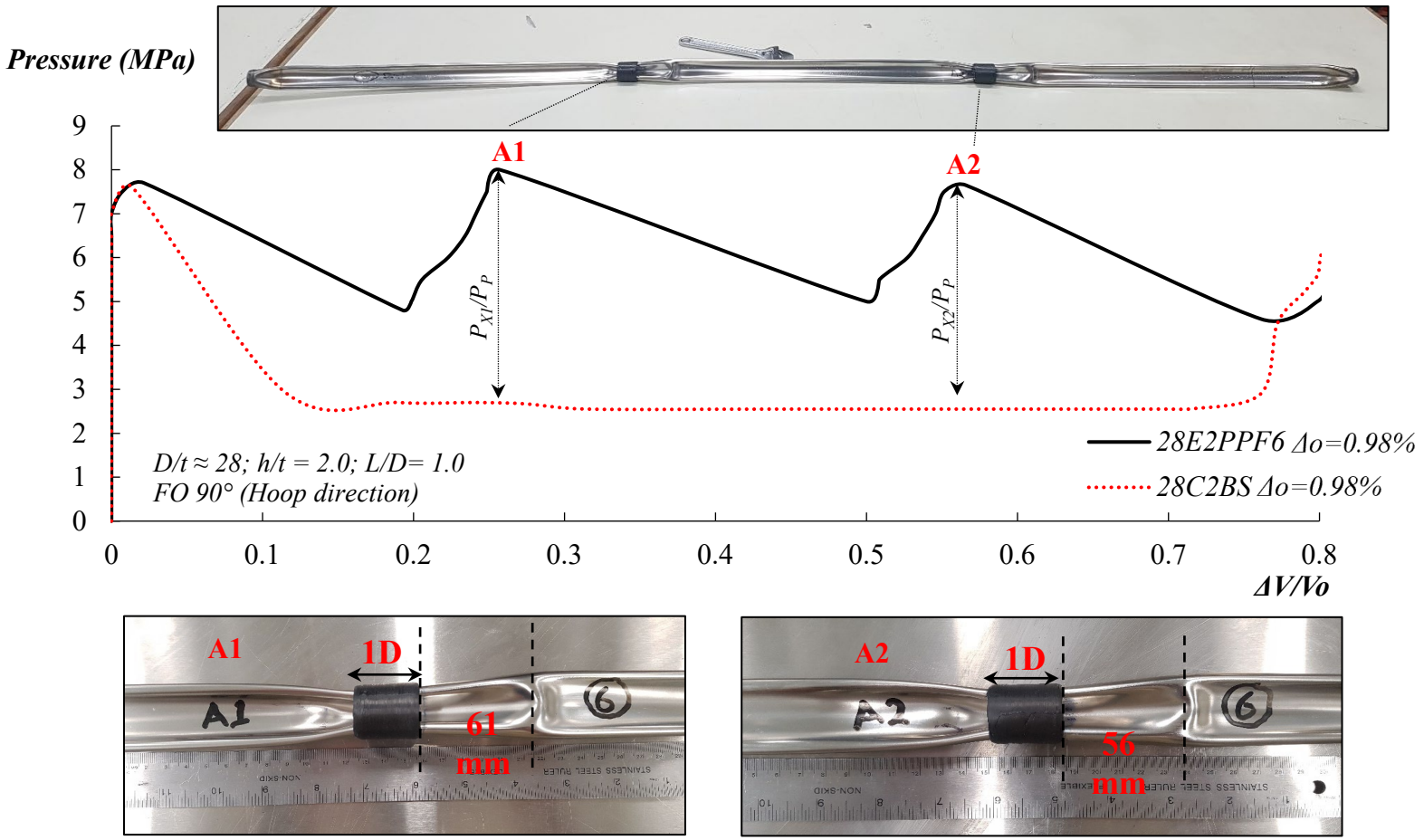

(b)

Fig.10. Pressure responses of; (a) sample 28E1PPF5, and (b) sample 28E2PPF6.

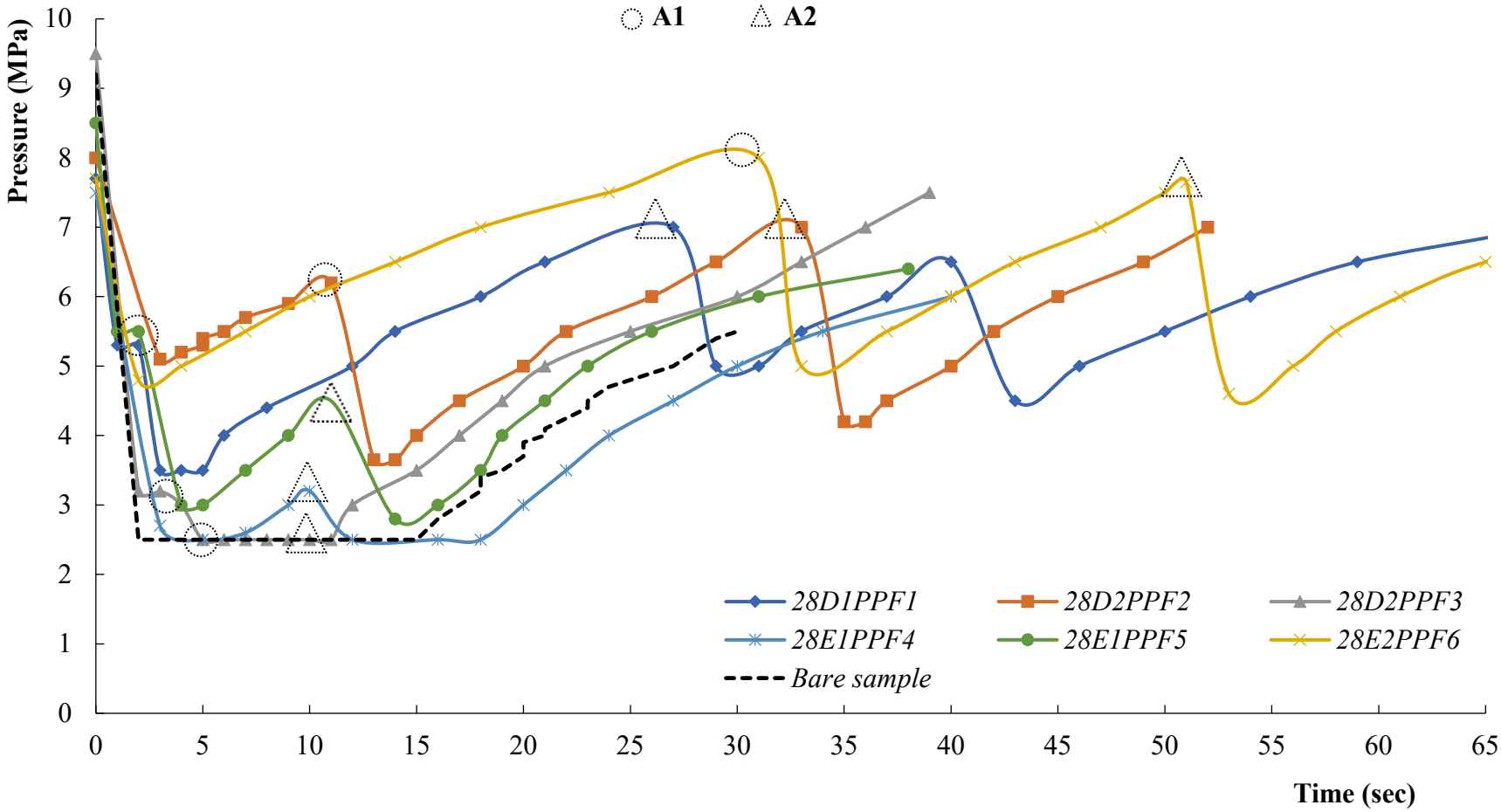

Fig.11. Pressure-time history of all samples from the parametric study (Test plan 2).

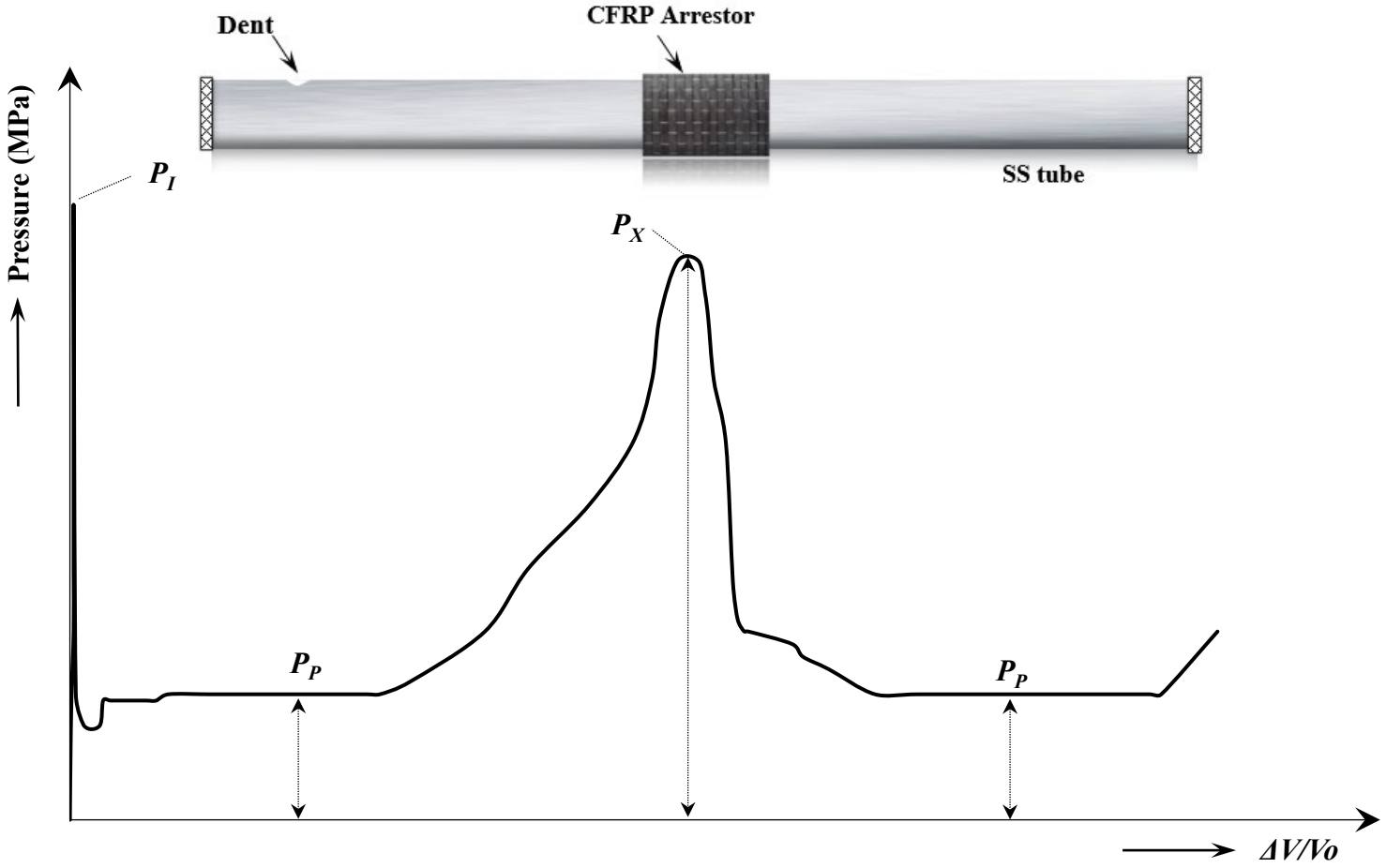

Fig.12. Schematic of pressure versus change of volume inside the hyperbaric chamber.

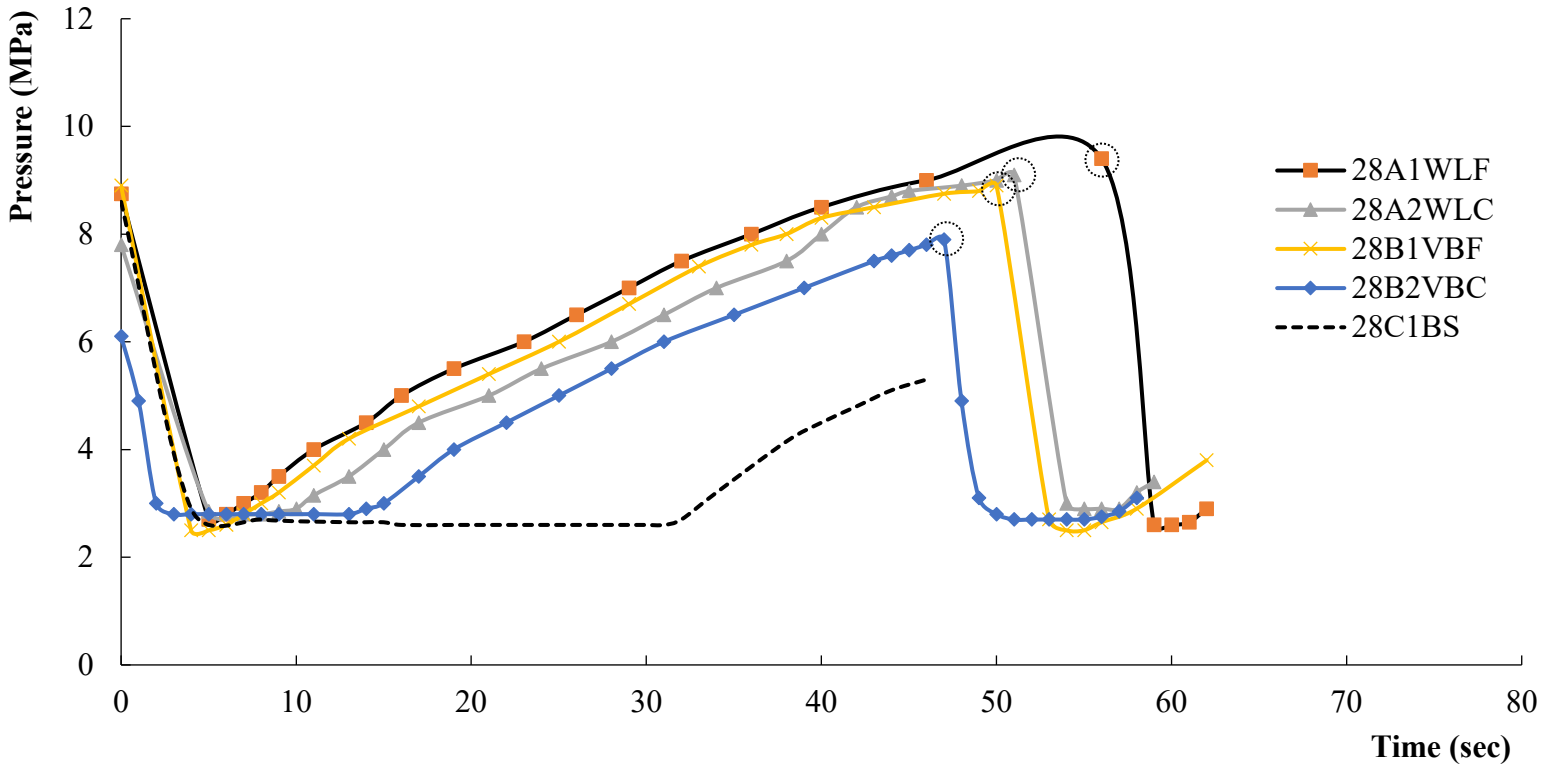
Pressure (MPa)
12
10
8
6
4
2
0
0
10
20
30
40
50
60
70
80
Time (sec)
28A1WLF
28A2WLC
28B1VBF
28B2VBC
28C1BS

(a)

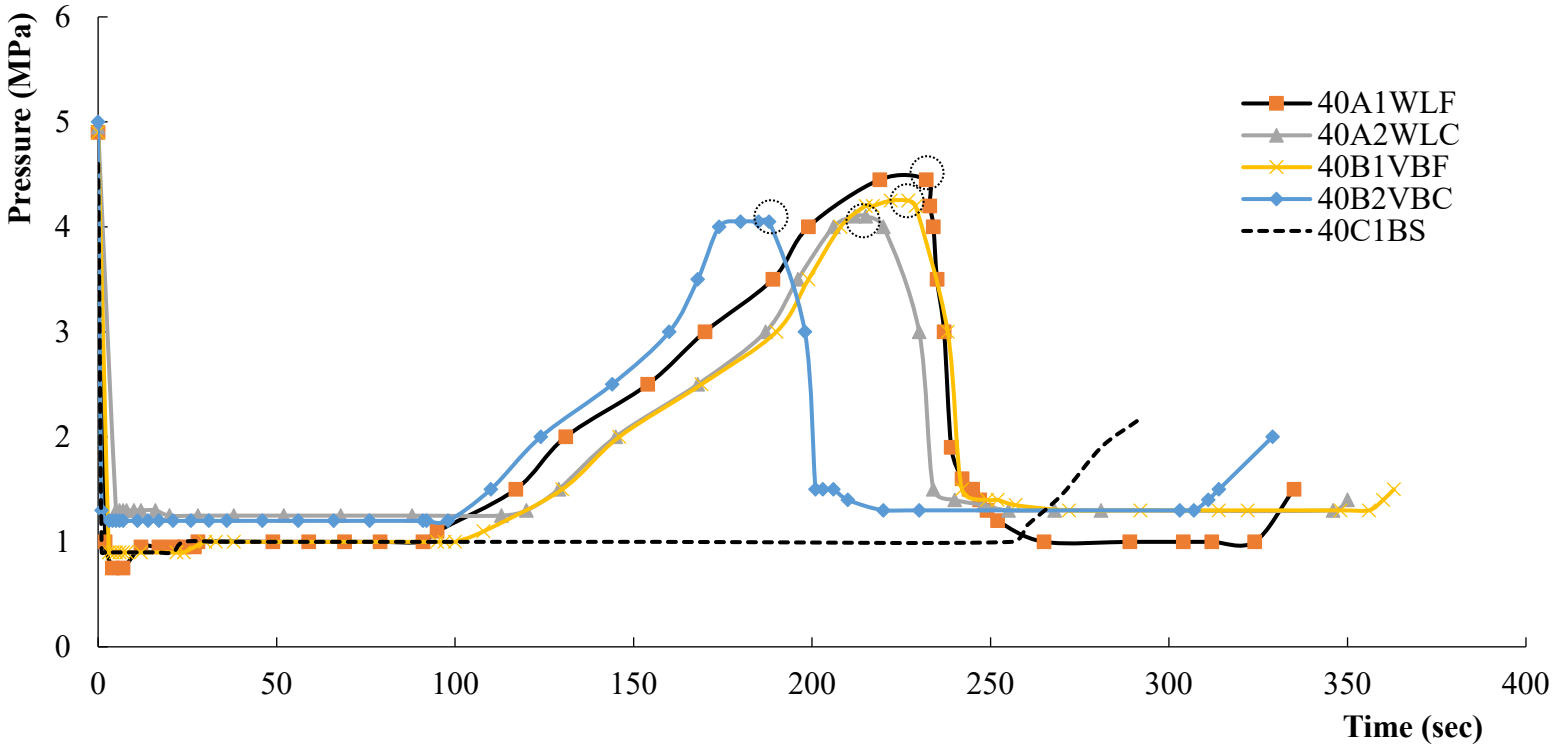

(b)

Fig. 13. Hyperbaric chamber pressure-time histories of test plan 3: (a) $D/t = 28$, (b) $D/t = 40$.

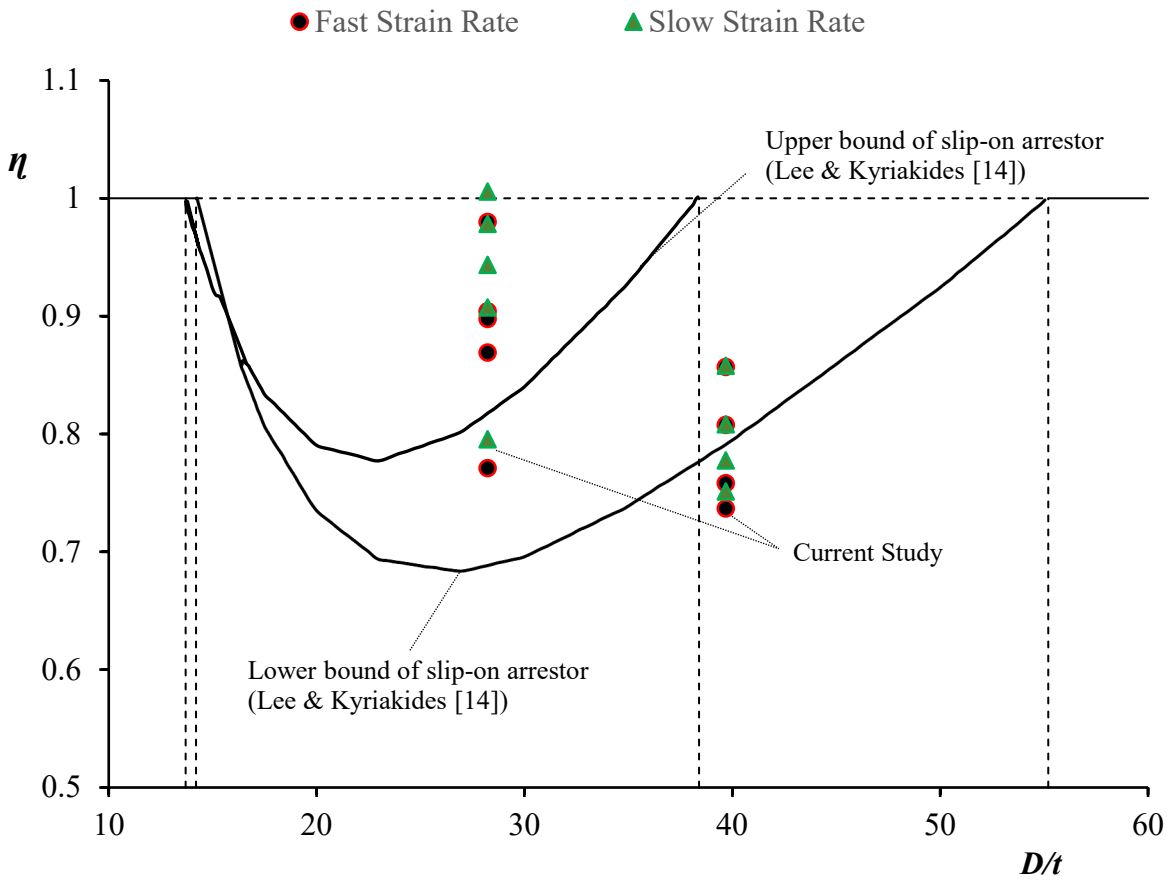

Fig. 14. Comparison between efficiency of the current CFRP arrestors (dot points) and slip-on arrestors [14] (lines).

Table 1. Coupon of the pipeline and results.

Coupon ID	Strain rate (s^{-1})×10^{-3}	D (mm)	t (mm)	E (GPa)	σ_y *0.2%* (MPa)	σ^L_y (MPa)	σ^U_y (MPa)	σ^L_u (MPa)	σ^U_u (MPa)	Elongation at Rupture (%)	P_P (Eq.7) (MPa)
28A1	2.667	25.4	0.9	207.6	348.3	437.0	444.5	679.7	692.0	64.2%	2.70
28A2	2.667	25.4	0.9	209.2	360.0	426.0	430.7	681.7	695.3	64.2%	2.79
28B1	2.667	25.4	0.9	199.9	357.3	402.5	407.4	655.2	672.2	64.2%	2.77
28B2	2.667	25.4	0.9	202.2	346.4	394.1	396.6	639.0	653.5	65.0%	2.69
28C1	0.333	25.4	0.9	208.9	337.4	382.3	386.2	642.9	655.0	65.6%	2.62
28C2	0.333	25.4	0.9	206.4	332.8	373.0	380.0	629.8	643.0	67.5%	2.58
28D1	0.333	25.4	0.9	196.2	341.2	387.7	388.0	662.2	672.2	66.5%	2.65
28D2	0.333	25.4	0.9	198.3	338.4	386.9	391.6	658.4	678.3	67.2%	2.62
28E1	0.333	25.4	0.9	209.6	340.1	385.3	389.0	654.2	666.9	68.1%	2.64
28E2	2.667	25.4	0.9	203.5	361.2	441.7	449.5	690.7	701.4	65.2%	2.80
40A1	0.733	63.5	1.6	201.0	311.2	337.7	340.0	674.2	685.3	88.3%	1.08
40A2	0.733	63.5	1.6	202.7	317.6	341.9	347.6	677.5	690.0	87.0%	1.10
40B1	0.733	63.5	1.6	198.9	316.5	351.0	354.3	687.0	697.6	88.5%	1.10
40B2	0.733	63.5	1.6	203.0	313.2	350.4	352.5	685.7	699.5	85.0%	1.09
40C1	0.093	63.5	1.6	204.6	301.8	322.3	326.7	684.4	694.3	91.7%	1.05
40C2	0.093	63.5	1.6	199.7	309.6	331.6	337.2	673.0	682.0	88.7%	1.07

Table 2. Coupon of the CFRP and average results.

Manufacturing Technique	Fiber Orientation	No. of Samples	E (GPa)	Ultimate Stress σ_u (MPa)	V_f
Prepreg (PP)	Longitudinal (0°)	3	132.7	1967.5	0.547
	Transverse (90°)	1	7.4	13.6	
Vacuum Bagging (VB)	Longitudinal (0°)	5	120.9	1854.9	0.513
	Transverse (90°)	3	7.6	25.27	
Wet Lay-up (WL)	Longitudinal (0°)	5	85.8	1310.4	0.350
	Transverse (90°)	3	5.5	27.7	

Table 3. Bare samples and the hyperbaric chamber results
(Test plan 1, Length of the tested pipeline is 2.5 meters).

Exp. ID	D (mm)	t (mm)	D/t	P_p (MPa)	P_I (MPa)	Pco (Eq.3) (MPa)	P_P (Eq.7) (MPa)
28C1BS	25.4	0.9	28.22	2.60	8.60	9.91	2.63
28C2BS	25.4	0.9	28.22	2.53	7.60	9.11	2.52
40C1BS	63.5	1.6	39.69	1.00	4.55	4.75	1.05
40C2BS	63.5	1.6	39.69	1.00	4.60	4.77	1.08

Table 4. Parametric study of CFRP and hyperbaric chamber results (Test plan 2, Length of the tested pipeline is 1.6 meters).

Exp. ID	CFRP Arrestor ID	*h/t*	*L/D*	Fibre Orientation (FO)	P_{Xi} (MPa)	$\left(\frac{P_{Xi}}{P_P}\right)$
28D1PPF1	1_A1	2.0	2.0	90°	5.3	2.08
	1_A2	2.0	2.0	90°	7.0	2.74
	1_A3	2.0	2.0	90°	6.5	2.55
28D2PPF2	2_A1	1.0	2.0	90°	6.2	2.43
	2_A2	1.0	2.0	90°	7.0	2.74
28D2PPF3	3_A1	1.0	2.0	35°	3.3	1.29
	3_A2	1.0	2.0	35°	2.5	1.00
28E1PPF4	4_A1	1.0	2.0	55°	2.7	1.06
	4_A2	1.0	2.0	55°	3.2	1.25
28E1PPF5	5_A1	1.0	1.0	90°	5.5	2.16
	5_A2	1.0	1.0	90°	4.5	1.76
28E2PPF6	6_A1	2.0	1.0	90°	8.0	3.14
	6_A2	2.0	1.0	90°	7.65	3.00

Table 5. Pipelines with CFRP arrestors and results
(Test plan 3, Length of the tested pipeline is 2.5 meters).

Exp. ID	D (mm)	t (mm)	D/t	Δ_0 (%)	h/t	L/D	P_P (MPa)	P_X (MPa)	$\frac{P_X}{P_P}$	$\frac{P_X}{P_I}$	Δt_d (s)
28A1WLF	25.4	0.9	28.22	0.994	2.0	2.0	2.70	9.40	3.48	1.07	56
28A2WLC	25.4	0.9	28.22	0.994	2.0	2.0	2.80	9.10	3.25	1.18	51
28B1VBF	25.4	0.9	28.22	0.994	2.0	2.0	2.60	8.85	3.40	1.00	50
28B2VBC	25.4	0.9	28.22	0.994	2.0	2.0	2.80	7.90	2.82	1.30	47
28E2PPF	25.4	0.9	28.22	1.250	2.0	1.0	2.55	8.00	3.14	1.04	31
40A1WLF	63.5	1.6	39.69	0.514	2.0	2.0	1.00	4.45	4.45	0.91	232
40A2WLC	63.5	1.6	39.69	0.514	2.0	2.0	1.20	4.15	3.46	0.84	215
40B1VBF	63.5	1.6	39.69	0.514	2.0	2.0	1.00	4.25	4.25	0.87	222
40B2VBC	63.5	1.6	39.69	0.514	2.0	2.0	1.20	4.05	3.37	0.81	188

Table 6. Efficiency of CFRP arrestors ($\theta = 90°$ in all)

Exp. ID	*D/t*	*h/t*	*L/D*	Strain rate (s^{-1}) $\times 10^{-3}$	σ_y *(0.2%)* (MPa)	*E* (MPa)	P_P (MPa)	P_X (MPa)	P_{co} *(Eq.3)* (MPa)	η_{CFRP}
28A1WLF	28.22	2.0	2.0	2.667	348.3	207.6	2.70	9.40	9.54	0.980
28C1WLF	28.22	2.0	2.0	0.333	337.4	208.9	2.70	9.40	9.36	1.006
28A2WLC	28.22	2.0	2.0	2.667	360.0	209.2	2.80	9.10	9.77	0.904
28C2WLC	28.22	2.0	2.0	0.333	332.8	206.4	2.80	9.10	9.24	0.978
28B1VBF	28.22	2.0	2.0	2.667	357.3	199.9	2.60	8.85	9.56	0.898
28D1VBF	28.22	2.0	2.0	0.333	341.2	196.2	2.60	8.85	9.23	0.943
28B2VBC	28.22	2.0	2.0	2.667	346.4	202.2	2.80	7.90	9.42	0.771
28D2VBC	28.22	2.0	2.0	0.333	338.4	198.3	2.80	7.90	9.21	0.795
28E2PPF6	28.22	2.0	2.0	2.667	361.2	203.5	2.55	8.00	8.82	0.869
28E1PPF6	28.22	2.0	2.0	0.333	340.1	209.6	2.55	8.00	8.56	0.907
40A1WLF	39.69	2.0	2.0	0.733	311.2	201.0	1.00	4.45	5.03	0.857
40C1WLF	39.69	2.0	2.0	0.093	301.7	204.6	1.00	4.45	5.02	0.858
40A2WLC	39.69	2.0	2.0	0.733	317.6	202.7	1.20	4.15	5.09	0.758
40C2WLC	39.69	2.0	2.0	0.093	309.6	199.7	1.20	4.15	5.00	0.777
40B1VBF	39.69	2.0	2.0	0.733	316.5	198.9	1.00	4.25	5.02	0.808
40C1VBF	39.69	2.0	2.0	0.093	301.8	204.6	1.00	4.25	5.02	0.808
40B2VBC	39.69	2.0	2.0	0.733	313.2	203.0	1.20	4.05	5.07	0.737
40C2VBC	39.69	2.0	2.0	0.093	309.6	199.7	1.20	4.05	5.00	0.751